Upregulated ectonucleotidases in FADD- and RIP1-deficient Jurkat leukemia cells counteract extracellular ATP/AMP accumulation via pannexin-1 channels during chemotherapeutic drug-induced apoptosis

Andrea M. Boyd Tressler, Graham S. Lane, and George R. Dubyak

Department of Physiology & Biophysics (GRD; GSL), Department of Pharmacology (AMB-T; GRD, Case Comprehensive Cancer Center (GRD), Case Western Reserve University School of Medicine, Cleveland OH 44106

Running title: *Ectonucleotidase modulation of apoptotic ATP/AMP accumulation*

Corresponding Author:
George R. Dubyak, Ph.D., Department of Physiology & Biophysics, School of Medicine, Case Western Reserve University, 10900 Euclid Avenue, Cleveland OH 44106. Telephone: (216)-368-5523; Email: george.dubyak@case.edu

Text pages: 32
Tables: 1
Figures: 8
References: 80
Abstract: 250 words
Introduction: 748 words
Discussion: 1517 words

Non-standard abbreviations: Staurosporine: STS; Etoposide: Etop; Tetramisole: Tetra; Prostatic Acid Phosphatase, transmembrane splice variant: TM-PAP; Tissue non-selective alkaline phosphatase: TNAP; Trovafloxacin: Trova; RIP: Receptor-interacting protein kinase; FADD: Fas-associated death domain protein; TRADD: TNF receptor-associated death domain protein; cIAP: cytosolic inhibitor of apoptosis; NSA: necrosulfonamide; Smac: second mitochondrial-derived activator of apoptosis; Pannexin-1: Panx1; Mixed lineage kinase-like protein: MLKL; α,β-methylene-ADP: APCP.

Abstract

Pannexin-1 (Panx1) channels mediate the efflux of ATP and AMP from cancer cells in response to induction of extrinsic apoptosis by death receptors or intrinsic apoptosis by chemotherapeutic agents. We previously described the accumulation of extracellular ATP /AMP during chemotherapy-induced apoptosis in Jurkat human leukemia cells. In this study, we compared how different signaling pathways determine extracellular nucleotide pools in control Jurkat cells versus Jurkat lines that lack the FADD or RIP1 cell death regulatory proteins. TNF-α induced extrinsic apoptosis in control Jurkat cells but necroptosis in FADD-deficient cells; treatment of both lines with chemotherapeutic drugs elicited similar intrinsic apoptosis. Robust extracellular ATP/AMP accumulation was observed in the FADD-deficient cells during necroptosis, but not during apoptotic activation of Panx1 channels. Accumulation of extracellular ATP/AMP was similarly absent in RIP1-deficient Jurkat cells during apoptotic responses to chemotherapeutic agents. Apoptotic activation triggered equivalent proteolytic gating of Panx1 channels in all three Jurkat cell lines. The differences in extracellular ATP/AMP accumulation correlated with cell-line specific expression of ectonucleotidases that metabolized the released ATP/AMP. CD73 mRNA and α.β-methylene-ADP-inhibitable ecto-AMPase activity were elevated in the FADD-deficient cells. In contrast, the RIP1-deficient cells were defined by increased expression of tartrate-sensitive prostatic acid phosphatase as a broadly acting ectonucleotidase. Thus, extracellular nucleotide accumulation during regulated tumor cell death involves interplay between ATP/AMP efflux pathways and different cell-autonomous ecto-nucleotidases. Differential expression of particular ectonucleotidases in tumor cell variants will determine whether chemotherapy-induced activation of Panx1 channels drives accumulation of immunostimulatory ATP versus immunosuppressive adenosine within the tumor microenvironment.

Introduction

The efficacy of cancer chemotherapy is enhanced by induction of sustainable anti-tumor immune responses. This is determined in part by accumulation of immunogenic mediators within the tumor micro-environment. These include bioactive peptides, lipids, and nucleotides released from cancer cells during chemotherapy- or receptor-induced activation of cell death signaling responses (Ghiringhelli et al., 2009; Gude et al., 2008; Kepp et al., 2009; Peter et al., 2012; Peter et al., 2008; Truman et al., 2008; Vacchelli et al., 2015; Zitvogel et al., 2008) . Given its high intracellular concentration, ATP comprises a ubiquitous tumor cell-derived immunogenic mediator. Extracellular ATP acts as a "find-me" signal for G protein-coupled P2Y-family receptors expressed on nearby macrophages and dendritic cells (DCs) (Chekeni et al., 2010; Elliott et al., 2009; Ma et al., 2013). This amplifies chemotaxis of these phagocytic leukocytes to the vicinity of dying cells and thereby facilitates the phagocytosis of tumor cells required for processing and presentation of tumor antigens to T lymphocytes.

Pannexin-1 (Panx1) channels comprise a major pathway for the regulated release of ATP to extracellular compartments in response to induction of either extrinsic apoptosis by death receptors or intrinsic apoptosis by chemotherapeutic agents (Boyd-Tressler et al., 2014; Chekeni et al., 2010). Apoptotic induction of active caspase-3 results in proteolytic excision of an autoinhibitory C-terminal segment to drive open-gating of the large-pore Panx1 channels and consequent efflux of intracellular metabolites such as ATP (Boyd-Tressler et al., 2014; Chekeni et al., 2010; Sandilos et al., 2012).

Several therapeutic agents, including agonists for TNF/TRAIL-family death receptors and various chemotherapeutic drugs, may induce regulated cancer cell death either by apoptosis or by necroptosis (Humphries et al., 2015; Martinou and Youle, 2011). The latter involves formation of necrosome complexes between RIP1 and RIP3 (receptor interacting protein kinases 1 and 3) to drive RIP3-mediated phosphorylation of the mixed-lineage kinase like (MLKL) pseudo-kinase. Phosphorylated MLKL (pMLKL) oligomerizes and inserts into the plasma membrane as multimeric pores with significant permeability to organic metabolites such as ATP (Humphries et al., 2015; Su et al., 2014; Sun et al., 2012; Wang et al., 2014; Wang et al., 2015). However, the relative kinetics and magnitudes of

extracellular ATP accumulation as mediated by RIP3-activated MLKL pores versus caspase-3-activated Panx1 channels in a given tumor cell model have not been quantified and compared.

Intrinsic apoptosis, extrinsic apoptosis, and necroptosis share several signaling nodes and regulatory proteins (Fig. 1A). TNF-α binding to type 1 TNF receptors (TNFR1) induces formation of "complex 1" containing the TRADD adapter, RIP1, and cIAP1/2 (cytosolic inhibitor of apoptosis proteins 1 and 2). This elicits NF-κB signaling and cell survival. However, when mitochondria release Smac (Second mitochondrial-derived activator of apoptosis) protein or when cells are treated with Smac-mimetic drugs the cIAPs are downregulated to facilitate the assembly of "complex 2" containing RIP1, FADD (Fas associated death domain) adapter, and caspase-8. Under these conditions, caspase-8 is activated to both initiate apoptosis and inactivate RIP1. However, if cells lacking FADD are treated with TNF-α and Smac-mimetic, complex 2 cannot assemble leaving RIP1 free to drive the RIP3/ MLKL necroptotic cascade. Riptosome signaling complexes, like "complex 2" platforms, contain RIP1, FADD, and procaspase-8, but also cFLIP, a protease-inactive caspase-8-like modulator protein. While FADD is best characterized for its roles in extrinsic apoptosis, the assembly of ripoptosomes can amplify death signaling by chemotherapeutic drugs that induce intrinsic apoptosis due to release of mitochondrial Smac and down-regulation of cIAPs (Belz et al., 2014; Feoktistova et al., 2011) (Tenev et al., 2011).

Although ATP directly released from dying tumor cells supports immunogenic anti-tumor responses by stimulating P2Y receptor signaling, it can also drive the generation of adenosine which activates immunosuppressive A2A/A2B receptors expressed on immune cells (Antonioli et al., 2013a; Stagg and Smyth, 2010). The balance between local ATP and adenosine accumulation within the tumor microenvironment will determine the net efficacy of anti-cancer immunogenic responses. Multiple studies have linked the decreased efficacy of cancer chemotherapies to increased levels of ectonucleotidases that metabolize released adenine nucleotides to adenosine (Beavis et al., 2012; Loi et al., 2013; Mikhailov et al., 2008). A wide range of ectoenzymes may differentially contribute to interstitial adenine nucleotide and adenosine levels in particular tumor environments (Table 1).

In this study, we compared how alternative pathways of nucleotide efflux and ectometabolism determine the composition of extracellular adenine nucleotide pools during death receptor-induced apoptosis or necroptosis versus chemotherapeutic drug-induced apoptosis in control Jurkat cells versus Jurkat variants lacking the FADD adapter protein or RIP1 kinase that modulate apoptotic and necroptotic cell death signaling responses.

Materials and Methods:

Cell Models and Reagents- The FADD deficient human Jurkat T cell acute leukemia cell line (I 2.1) and the wild-type human Jurkat T cell acute leukemia cells were obtained from ATCC (Manassas VA). The RIP1 deficient human Jurkat T cell acute leukemia cell line was generously provided by Zheng-gang Liu (National Cancer Institute, Bethesda MD) (Morgan et al., 2009). BV6 was provided by Genentech (South San Francisco CA. Other key reagents were purchased from commercial vendors. Human recombinant TNF-α was from PeproTech (Rocky Hill NJ). zVAD-fmk and pentostatin (2-deoxycoformycin) were from APExBio (Houston TX). Necrosulfonamide (NSA) and ARL67156 were from Tocris (Minneapolis MN). Anti-human Fas (CH11 clone) was from Millipore (Billerica MA). Staurosporine was from LC Laboratories (Woburn MA). Lyophilized Firefly Luciferase ATP Assay Mix (FLAAM), Firefly Luciferase ATP Assay Buffer (FLAAB), pyruvate kinase (P-1506), myokinase (M-3003), ATP, 1,N6-etheno-AMP, phosphoenolpyruvate, etoposide, tetramisole, trovafloxacin, L-tartaric acid (Na salt), TRIzol reagent, and DAPI stain were from Sigma-Adrich (St. Louis MO). Calcein-AM, YOPRO, and MitoTracker® Red CM-H_2XRos were from Invitrogen (Carlsbad CA). The cytotoxicity detection kit (LDH release) was from Roche Applied Science (Indianapolis IN). Anti-PARP (9542) was from Cell Signaling (Danvers MA). Anti-PAP was from R&D (Minneapolis MN). AllinOne ™ FirstStrand cDNA Synthesis Kit, AllinOne ™ qPCR Mix, CD73 qPCR primers, and GAPDH qPCR primers were from GeneCopoeia (Rockville MD). Anti-β actin (sc-1615) and all horseradish peroxidase (HRP)-coupled secondary antibodies were from Santa Cruz Biotechnology (Dallas TX). Pierce® ECL Western blotting substrate was from ThermoFisher Scientific (Waltham MA). αβ-methylene-adenosine 5'-diphosphate (APCP) was from Jena Bioscience (Jena, Germany). The specificity of the noncommercial rabbit anti-human pannexin-1 antiserum has been described previously (Boyd-Tressler et al., 2014; Chekeni et al., 2010; Penuela et al., 2007; Penuela et al., 2009).

Cell culture and induction of apoptosis and necroptosis – Wildtype, FADD-deficient, and RIP1-deficient Jurkat cells were maintained in RPMI-1640 media supplemented with 10% newborn bovine calf serum

(Hyclone –GE Healthcare BioSciences, Pittsburgh PA), 100 units/ml penicillin, 100 µg/ml streptomycin (Invitrogen, Carlsbad CA), and 2 mM L-glutamine (Lonza, Basel Switzerland) at 37°C in 5% CO2. For induction of apoptosis and analysis of released adenine nucleotides, the wildtype Jurkat cells were resuspended at $2x10^6$ cells/ml (2 ml/well; 12-well plates) in RPMI-1640 as above but with 10% bovine calf serum treated for 2 h at 65°C to inactivate serum nucleotidases. For TNF-α induced apoptosis, the resuspended cells were pre-incubated with 3µM BV6 for 2 hours at 37°C in 5% CO_2 prior to addition of 20ng/mL TNF-α. Apoptosis in all Jurkat cell types was induced by 3µM STS, 20µM etoposide, or 250ng/mL anti-Fas. For induction of necroptosis, FADD deficient Jurkat cells were resuspended at $2x10^6$cells/mL and pre-incubated with 3µM BV6 for 2 hours at 37°C in 5% CO_2 prior to addition of 20ng/mL TNF-α. Where indicated, 20µM, 50µM, or 100µM zVAD, 1µM NSA, or 30µM Trovafloxacin were added to the cell cultures 1 hour prior to addition of TNF-α, Anti-Fas, STS, or Etop. Where indicated, 50µM APCP was added 10 min prior the addition of TNF-α, Anti-Fas, STS, or Etop.

Collection of conditioned medium and measurement of released adenine nucleotides - Conditioned medium from control, apoptotic, or necroptotic Jurkat cells was collected and assayed for accumulation of extracellular adenine nucleotides as described previously (Boyd-Tressler et al., 2014). Briefly, samples of the conditioned medium supernatants were taken at indicated times (routinely 0, 2, 4, 8, 12 h) after addition of TNF-α, anti-Fas, STS, or Etop and centrifuged at 13,500 RPM for 15 sec to pellet cells. The cell-free supernatants were transferred to fresh tubes for analysis of either ATP only or total adenine nucleotides (ATP + ADP + AMP). For luciferase-based quantification of ATP only, a 50 µL aliquot of conditioned medium supernatant was supplemented with 46 µL of FLAAB and 4 µL of concentrated FLAAM (reconstituted with 5 ml sterile water per vial of lyophilized luciferase/luciferin mix) and transferred to a well of a 96-well white plate. The ATP-dependent bioluminescence was measured with a BioTek Synergy HT plate reader (1 second integration of emitted light) and quantified by comparison to ATP standards assayed under identical conditions. For quantification of total adenine nucleotides, samples were subjected to a protocol modified from that described in (Hampp, 1985) whereby AMP and

ADP were rephosphorylated to ATP (in a cycling reaction driven by excess phosphoenolpyruvate (PEP) in the presence of pyruvate kinase and myokinase) prior to the luciferase analysis described above. 50 μL of conditioned medium supernatant was supplemented with 8.3μL of rephosphorylation cocktail (25mM K-HEPES, pH 8.0, 50mM MgSO4, 8.3 mM PEP, 600U/mL myokinase, 300U/mL pyruvate kinase) and incubated for 90 min at 37°C. 37.7 μL FLAAB and 4 μL concentrated FLAAM were then added to each rephosphorylated sample and ATP-dependent bioluminescence was measured.

Measurement of Cell Lysis by LDH Release- Cells were treated with apoptotic or necroptotic stimuli as described above. After brief centrifugation of the cell suspensions, the cell-free supernatants were assayed for LDH enzyme activity using the cytotoxicity detection kit according to the protocol of Roche Applied Science. The released LDH was normalized to total LDH content measured in 1% Triton X-100-permeabilized samples of untreated Jurkat T cells.

Western Blot Analyses - 1 ml aliquots of 2 x 10^6 Jurkat cells were centrifuged and the cell pellets were washed in PBS. Whole cell lysates were prepared by detergent-based extractions prior to standard processing by SDS-PAGE (either 12% or 4-20% polyacrylamide), transfer to PVDF membranes, and western blot analysis as described previously (Boyd-Tressler et al., 2014). Primary antibodies (Abs) were used at the following concentrations or dilutions: anti-human pannexin 1 (1:5000), anti-PARP (1:1000), anti-β-actin (1 μg/ml), or anti-PAP (1 μg/ml). HRP conjugated secondary Abs were used at a final concentration of 0.13 μg/ml. Chemiluminescent images of the blots were developed with ECL reagent, imaged, and quantified using a FluorChemE processor and AlphaView SA imaging software (Cell Biosciences).

YO-PRO Dye Influx - 500μL aliquots of Jurkat cell suspension (10^6/ml) were treated with apoptotic stimuli as described above for various times, collected by centrifugation, and washed once with PBS. The washed cell pellets were resuspended in 500 μL of basal salt solution (BSS) containing 130 mM NaCl, 5 mM KCl, 1 mM $MgCl_2$, 1.5 mM $CaCl_2$,25 mM NaHEPES, pH 7.5, 5 mM glucose, and 0.1% bovine serum albumin. 1 μM YO-PRO dye was added and the cells were incubated for 20 min. The cells were

then pelleted by brief centrifugation, washed once in PBS, and resuspended in 500 µl fresh BSS. 200 µl aliquots were transferred to wells in a 96-well plate and the fluorescence (485nm/540 nm) was measured on the BioTek Synergy HT plate reader. Phase-contrast and epifluorescence images of the cells in each well were then recorded using a Zeiss Axiovert 25 Microscope equipped with a 485 nm/540 nm filter set, QCam1394 digital camera, and QCapturePro imaging software (QImaging, Surrey BC, Canada).

Calcein Dye Efflux- Jurkat cells were suspended at $2x10^6$cells/mL in RPMI+10% heat inactivated calf serum+100 units/ml penicillin, 100 µg/ml streptomycin, and 2 mM L-glutamine. The suspensions were supplemented with 1µM calcein-AM and 250µM probenecid and incubated for 45 minutes at 37°C. Cells were washed in PBS, resuspended in the same RPMI test medium, and then treated with 3µM STS in the presence or absence of 100µM zVAD or 30µM Trovafloxacin for 4 hours at 37°C and 5% CO_2. After brief centrifugation, the cell pellets were washed and resuspended in BSS+5mM Glucose+0.1% BSA and the fluorescence (485nm/528nm) was measured on the BioTek Synergy HT plate reader.

Imaging of Mitochondrial Localization - $1x10^6$ Jurkat cells/mL were incubated for 4 h with or without 3 µM STS. The cells were pelleted, washed with PBS, and resuspended in pre-warmed (37°C) staining solution consisting of 500nM MitoTracker® Red CM-H_2XRos in BSS+5mM Glucose+0.1%BSA and incubated for 30 minutes at 37°C in the dark. Cell were pelleted, washed in PBS, resuspended in BSS+5mM glucose+0.1% BSA supplemented with a 1:100 dilution of DAPI (0.2ug/mL working stock), and incubated in the dark at room temperature for 5-10 minutes. Cells were pelleted, washed in PBS,fixed in 200µL of 4% Paraformaldehyde in PBS for 15 minutes at 37°C. The fixed cells were repelleted, washed, and resuspended in 50µL 0.5% paraformaldehyde and stored at 4°C. Images of the cells were acquired using an Olympus FluoView™ FV1000 laser scanning confocal microscope coupled with an IX-81 inverted microscope equipped with a 60×/1.42 NA oil immersion objective and a computer running FluoView™ FV10-ASW Ver. 3.1b software (Olympus America Inc., Center Valley, PA).

Extracellular ATP and AMP hydrolysis assays- Wild-type, FADD-deficient, or RIP1-deficient cells were resuspended at $2x10^6$ cells/mL in the RPMI assay medium for assay of extracellular AMP hydrolysis or in

BSS+5mM glucose+0.1% BSA for assay of extracellular ATP hydrolysis. After addition of 1μM AMP or ATP, the cell suspensions were incubated for 30 min at 37°C, and then centrifuged at 13,500 RPM for 15 sec to pellet cells. The cell-free supernatants were collected and assayed for ATP or AMP by the luciferase-based methods described above. Where indicated, 50μM APCP, 5 mM tetramisole, 200 μM pentostatin or 100μM ARL67156 was added to the cell suspension 10 min prior to addition of AMP or ATP.

HPLC assays of extracellular AMP metabolism and adenosine/inosine accumulation or extracellular etheno-AMP metabolism and etheno-adenosine accumulation- Wild-type, FADD-deficient, or RIP1-deficient cells were suspended at $2x10^6$ cells/mL in BSS+5mM Glucose+0.1%BSA and pre-incubated for 15min at 37°C. The cell suspensions were supplemented with 10 μM 1, N6-etheno-AMP (ε-AMP) or 100 μM AMP plus or minus various inhibitors as indicated, incubated for 30 min at 37°C, and then centrifuged at 13,500 RPM for 15 sec. The cell-free supernatants were transferred to new tubes, boiled for 5 min at 100°C, and then placed on ice. Extracellular ε-AMP and etheno-adenosine (ε-ADO) were resolved by and quantified by ion exchange HPLC using a Bio-Rad Gradient Module HPLC connected to a Linear™ Fluor LC305 fluorescence detector. Samples were diluted 1:10 in water and 50 μL injected onto a Hamilton PRP-X100 anion exchange column which was eluted at 1.0 or 1.6 mL/min with a gradient of NH_4HCO_3 in 30% methanol. The baseline mobile phase was 0.25 M NH_4HCO_3 (pH 8.5) in 30% methanol. After sample injection, the mobile phase was developed linearly from 0.25 to 0.275 M NH_4HCO_3 for 8 min, remained isocratic at 0.275 M NH_4HCO_3 for the next 4 min, washed for 3 min at 0.425 M NH_4HCO_3 and then re-equilibrated back to the baseline mobile phase for 15 min. Extracellular AMP, IMP, adenosine, and inosine were resolved by reverse HPLC using a Bio-Rad Gradient Module HPLC connected to an absorbance detector. Samples were diluted 1:10 in water and 50 μL injected onto a Alltech C18 Nucleotide/Nucleoside reverse phase column which was eluted at 1.0 mL/min with a gradient of methanol in 20mM $(NH_4)_3HPO_4$ (pH 6). The baseline mobile phase was 20mM $(NH_4)_3HPO_4$ (pH 6) in 0% methanol. After sample injection, the column was eluted with isocratic 0% methanol for 4

min followed by an gradient increase to 8% methanol from 4-6 min, a gradient increase 20% methanol from 6-8 min, isocratic elution with 20% methanol from 8-18 min, a gradient decrease to 0% methanol form 18-20 min, and then isocratic elution with 0% methanol to re-equilibrate the column to the baseline condition. Absorbance of eluate was continuously recorded at 260 nm. Injection with standard solutions of 100 μM IMP, AMP, inosine, or adenosine were used to identify the retention time of those nucleotides and nucleosides. Chromatogram peaks were obtained with Data Ally v2.06 software.

Assay of ecto-nitrophenyl phosphatase activity in Jurkat cells: 200 μl aliquots of wildtype, RIP1-deficient, and FADD-deficient Jurkat cells (2 x10^6/ml) were plated in 96-well plates. The cells were suspended in BSS (+ glucose and BSA) that was buffered to pH7.5 or pH 6.5. The cell suspensions were supplemented with 500 μM *p*-nitrophenyl phosphate, in the absence or presence of 10 mM L-tartrate (sodium salt) or 50μM APCP, and incubated for 3h at 25°C. Hydrolysis of nitrophenyl phosphate to nitrophenyl was assayed by measuring absorbance at 405 mm on the BioTek Synergy HT plate reader.

qPCR analysis of CD73 expression - Total RNA was extracted by TRIzol reagent from wildtype, FADD-deficient, or RIP1-deficient Jurkat cells by standard methods. All-in-One™ First-Strand cDNA Synthesis kit was utilized for synthesis of first-strand cDNA from purified RNA. Quantitative PCR (qPCR) analysis of CD73 or GAPDH mRNA was performed using a StepOne-Plus Real-Time PCR System (Applied Biosystems). Reactions were performed in 20 μl reaction volumes containing All-in-One™ qPCR Mix with ROX reference dye, 0.2 μM PCR primers, 1:100 dilution of the first strand cDNA reaction, and run in triplicate. Relative expression was calculated using the $\Delta\Delta C_t$ method using StepOne software v. 2.1 with values normalized to the reference gene GAPDH; relative differences in CD73 mRNA levels in FADD-deficient or RIP1-deficient cells were normalized to the values in measured in wildtype Jurkat cells.

Data Analysis - Experiments were repeated 3-6 times with separate Jurkat cell culture preparations. Western blot results are from representative experiments. Figures illustrating quantification of extracellular adenine nucleotide accumulation, LDH release, extracellular nucleotide hydrolysis, YO-PRO

dye influx, calcein dye efflux represent the mean (± SE) of data from 3-6 independent experiments each performed with 2-4 technical replicates. Quantitative results were analyzed by T-test or two-way ANOVA with Tukey post-test comparison using Prism 6.0 software.

Results

TNFα-induction of necroptosis or extrinsic apoptosis induces release of adenine nucleotides from Jurkat cells via mechanistically distinct pathways

T cell leukemias or lymphomas have been widely used as tumor cell models for examining the relationships between Panx1-mediated ATP release, extracellular ATP/AMP metabolism, adenosine accumulation, and the modulation of anti-tumor immune responses in vivo and in vitro (Chekeni et al., 2010; Elliott et al., 2009; Ghiringhelli et al., 2009; Martins et al., 2009; Poon et al., 2014). We previously described roles for Panx1 channels in the release of both ATP and AMP during chemotherapeutic drug-induced apoptosis of Jurkat human leukemic T cells (Boyd-Tressler et al., 2014). In wildtype (WT) Jurkat human leukemic T cells, TNF-α (T) binding to type 1 TNF receptors (TNFR1) induces formation of complex 1 signaling platforms. However, when these cells are treated with Smac mimetic drugs such as BV6, the cIAPs are downregulated to facilitate the assembly of complex 2. Under these conditions, caspase-8 is activated to both initiate apoptosis and inactivate RIP1. Conversely, when Jurkat cells deficient in FADD (FADD-deficient) are treated with TNF-α plus BV6, complex 2 cannot assemble leaving RIP1 free to form necrosome platforms that license RIP3-dependent MLKL pore formation and necroptosis. Fas receptor-induced apoptosis of WT Jurkat cells has been previously shown to elicit ATP efflux via caspase-3-mediated cleavage of the C-terminus of Panx1 channels (Fig. 1A). While the kinetics and magnitude of this Fas-induced ATP release from Jurkat cells has been defined (Chekeni et al., 2010), it is not known whether similar Panx1 cleavage and ATP efflux parameters characterize TNFR1-induced apoptosis or how MLKL pores may facilitate alternative ATP efflux parameters during TNFR1-induced necroptosis.

Using WT and FADD-deficient Jurkat cells identically co-treated with TNFα plus BV6 Smac mimetic, we compared the kinetics of lytic plasma membrane disruption (as indicated by release of the cytosolic macromolecule lactate dehydrogenase, LDH) during apoptotic versus necroptotic progression. While WT cells treated with TNFα plus BV6 for up to 12 h did not release LDH (Fig. 1B), FADD-

deficient cells began to release LDH within 4 h and this progressively increased to ~60% cell lysis by 12 h (Fig. 1C). The TNFα plus BV6-induced lysis of FADD-deficient cells was completely suppressed by necrosulfonamide (NSA), an inhibitor of the phosphorylated MLKL oligomerization necessary for insertion of MLKL pores into the plasma membrane (Sun et al., 2012). In contrast, there was no attenuation of LDH release from FADD-deficient cells treated with TNFα plus BV6 in the presence of the pan-caspase inhibitor zVAD (Fig. 1C). These observations confirm that TNF-α induced necroptotic signaling is defined by rapid plasma membrane disruption independently of apoptotic caspases and that TNF-α induced apoptotic signaling over a similar 12 h test period does not result in secondary necrosis.

Despite these marked differences in lytic plasma membrane disruption, TNFα plus BV6 induced similar extracellular adenine nucleotide accumulation (1-1.5 μM at 8-12 h) by the WT and FADD-deficient Jurkat cells cultured at $2x10^6$/ml. We characterized the kinetics and underlying apoptotic mechanism of TNFα plus BV6-induced adenine nucleotide release from the WT cells by using Fas receptor activation as a positive control and measuring the summed accumulation of extracellular ATP, ADP and AMP (ATP+ADP+AMP). Our previous study (Boyd-Tressler et al., 2014) determined that analysis of ATP+ADP+AMP, rather than ATP alone, provides a better readout of net Panx1 channel-mediated adenine nucleotide efflux during apoptotic progression because the intracellular nucleotide pool shifts from initially high [ATP] and low[ADP]+[AMP] to lower [ATP] and higher [ADP]+[AMP] as a consequence of the increased ATP utilization and decreased mitochondrial ATP synthesis that characterizes apoptotic signaling (Ricci et al., 2004; Waterhouse et al., 2001). TNFα plus BV6-induced apoptosis resulted in a steady and significant increase in ATP+ADP+AMP after ~ 4 h lag time and this was suppressed in the presence of zVAD but not NSA (Fig 1E). These ATP+ADP+AMP accumulation responses were similar to those observed in αFas-treated WT Jurkat cells but with modestly slower kinetics (Fig 1D). In both TNFα plus BV6- and αFas-treated WT Jurkat cells, the time course of the ATP+ADP+AMP accumulation correlated with the activation of caspase-3 as indicated by cleavage of the canonical substrate poly-ADP-ribose polymerase (PARP) (Figs. 1G and H).

We also compared the proteolytic processing of Panx1 channels during the TNFα plus BV6- versus αFas-treatments. Panx1 exists in three different glycosylation states: unglycosylated Gly-0, monoglycosylated Gly-1, and Gly-2 which is the fully glycosylated and most abundant form that accumulates in the plasma membrane as a 48-50 kDa protein (Penuela et al., 2007; Penuela et al., 2013). All three forms are detected using a previously characterized polyclonal antibody that recognizes the extreme intracellular C-terminus of Panx1 downstream of the caspase-3 cleavage site (Boyd-Tressler et al., 2014; Chekeni et al., 2010). Caspase3-mediated cleavage of Panx1 during apoptotic progression results in a decreased anti-Panx1 48-50 kDa band on western blots of whole cell lystates due to loss of the antibody binding site. Panx1 cleavage was evident within 4 h in αFas-treated WT cells and within 8 h in the TNFα plus BV6-treated cells (Fig 1G and H). These data, together with the observed lack of LDH release, indicate that the ATP+ADP+AMP accumulation triggered during TNF-receptor mediated apoptosis is mediated by efflux through caspase-3-activated Panx1 channels prior to secondary necrosis. This confirms that engagement of multiple death receptors in Jurkat leukemia activates similar extrinsic apoptotic signaling programs leading to proteolytic gating of Panx1 channels that mediate efflux of cytosolic ATP, ADP, and AMP pools.

In contrast to the WT cells, FADD-deficient Jurkat cells responded to TNFα plus BV6 with robust ATP+ADP+AMP accumulation that started at 2 h and peaked at 8 h. This response was completely suppressed by NSA but insensitive to zVAD (Fig 1F) indicating that extracellular adenine nucleotide accumulation was dependent on insertion of non-selective MLKL pores into the plasma membrane. Also consistent with this mechanism, no obvious cleavage of PARP or Panx1 was evident in TNFα plus BV6-stimulated FADD-deficient Jurkat cells at the 4- and 8 h-time points coinciding with significant nucleotide release (Fig. 1I). It is important to note that the decrease in the Panx1 (and uncleaved PARP1) western blot signals occurring after 8h is due to loss of viable cell mass as indicated by the decreased actin signal. Taken together, these data from FADD-deficient Jurkat cells indicate that although TNFR1 signaling is redirected from extrinsic apoptosis to necroptosis, this regulated cell death

results in extracellular accumulation of ATP, ADP and AMP released via MLKL pores concurrent with cell lysis.

Intrinsic apoptotic signaling and Panx1 channel cleavage in FADD-deficient Jurkat cells are uncoupled from accumulation of extracellular adenine nucleotides

Although FADD is a critical mediator of extrinsic apoptosis by Fas or TNFR1, the assembly of RIP1/FADD/caspase-8 ripoptosomes also amplifies intrinsic apoptosis triggered by chemotherapeutic drugs due to release of mitochondrial Smac and down-regulation of IAPs (Belz et al., 2014; Feoktistova et al., 2011). We tested whether the absence of FADD modulated Panx1-mediated accumulation of extracellular adenine nucleotides in Jurkat cells stimulated with chemotherapeutic drugs. We previously reported that multiple chemotherapeutic or pro-apoptotic drugs, including staurosporine (STS) and etoposide (Etop), trigger caspase-3-mediated activation of Panx1 channels and consequent adenine nucleotide efflux in WT Jurkat T cells (Boyd-Tressler et al., 2014). Using these responses in WT cells as positive controls, we similarly treated FADD-deficient Jurkat cells with STS or Etop for up to12 h and assayed Panx1 and PARP cleavage (Figs. 2A, B), secondary necrosis (Figs. 2C, D), and ATP+ADP+AMP accumulation (Figs. 2E, F). Both STS and Etop induced robust intrinsic apoptosis in the FADD-deficient cells as indicated by cleavage of PARP and Panx1 with similar kinetics compared to the responses in WT cells. We verified that the FADD-deficient Jurkat cells were unable to undergo extrinsic apoptosis as indicated by the absence of PARP and Panx1 cleavage in response to αFas (Fig 2B). STS induced near-maximal apoptotic activation within 4-6 h in both Jurkat lines while significant responses to Etop required a 6-8h exposure. Secondary necrosis was observed when either cell line was treated with STS (Fig. 2C-i; Fig.2D-i), but not Etop (Fig. 2C-ii; Fig.2D-ii), for >8h; this lytic release of LDH was completely suppressed by zVAD.

Consistent with our previous findings (Boyd-Tressler et al., 2014), STS (Fig. 2E-i) and Etop (Fig. 2E-ii) induced robust ATP+ADP+AMP accumulation in WT Jurkat cells that was: 1) temporally correlated with the kinetics of Panx1 proteolytic processing (Fig. 2A); 2) insensitive to NSA; and 3)

markedly suppressed by zVAD. We previously demonstrated that the zVAD-insensitive component of nucleotide release in STS-treated Jurkat cells is insensitive to blockade of Panx1 channels but suppressed by intracellular Ca^{2+} buffering (Boyd-Tressler et al., 2014). To our surprise, very little extracellular extracellular ATP+ADP+AMP accumulation was observed in the FADD-deficient Jurkat cells treated with STS (Fig. 2F-i) or Etop (Fig. 2F-ii) despite the robust proteolytic processing of Panx1 channels. These data indicate that FADD deficiency uncouples accumulation of extracellular adenine nucleotides from caspase-3-mediated cleavage and activation of Panx1 channels.

Caspase-3-cleaved Panx1 channels are functionally active in FADD-deficient Jurkat cells during intrinsic apoptosis

The decreased extracellular accumulation of ATP+ADP+AMP by apoptotic FADD-def Jurkat cells might reflect: 1) lack of functional Panx1 channels; 2) altered ion selectivity or rectification properties of active Panx 1 channels; 3) altered localization of ATP-producing mitochondria within the local membrane environment of active Panx1 channels; or 4) increased ecto-nucleotidase activity. As illustrated in Fig. 3A, caspase-3-mediated excision of the C-terminal autoinhibitory domains of Panx1 channels gates their permeability as ATP efflux conduits, but also as influx/efflux pathways for normally impermeant organic dyes. To test whether caspase-3-processed Panx1 channels are functionally blocked in apoptotic FADD-deficient Jurkat cells, we adapted our previously described assay (Boyd-Tressler et al., 2014) for the influx of YO-PRO^{2+}, a 375-Da divalent cationic dye that intercalates with DNA to produce green fluorescence.

WT or FADD-deficient cells (control and apoptotic) were pulsed with extracellular YO-PRO^{2+} at times corresponding to maximal Panx1 cleavage by STS (4 h) or Etop (12 h), and dye uptake was quantified by fluorescence plate reader analysis (Fig. 3B) and visualized by fluorescence microscopy (Fig. 3D). Significant increases in YO-PRO^{2+} dye uptake were observed in both WT and FADD-deficient cells treated with STS relative to untreated controls for each cell line (Fig. 3B). Although the quantified magnitude of YO-PRO^{2+} accumulation was modestly lower in the apoptotic FADD-def cells relative to

apoptotic WT cells, these data indicate that intrinsic apoptosis does induce accumulation of functionally active Panx1 channels in the FADD-deficient Jurkat cells. However, this assay of Panx1 function measures the influx of an organic cation while ATP/AMP are organic anions that efflux from the cell. To test whether FADD deficiency might alter the ion selectivity or rectification properties of Panx1 channels, we loaded WT or FADD-deficient Jurkat cells with the anionic calcein^{4-} dye prior to the 4 h treatment with STS. Similar amounts of calcein^{4-} were released from the apoptotic WT and FADD-deficient cells (Fig 3C). We confirmed that this calcein^{4-} efflux was mediated by caspase-3-activated Panx1 channels by performing parallel measurements in the presence of zVAD or the Panx1 channel blocker trovafloxacin (Trov) (Poon et al., 2014). Both inhibitors caused complete retention of calcein^{4-} within the WT and FADD-deficient cells during STS treatment. These results indicate that changes in Panx1 channel ion selectivity, conductance, or rectification are unlikely mechanisms for the marked suppression of extracellular adenine nucleotide accumulation in FADD-deficient Jurkat cells.

FADD deficiency does not alter mitochondrial localization in control or apoptotic Jurkat cells

Recent studies have reported that, during T cell activation, mitochondria translocate to the plasma membrane subdomains of the immune synapse resulting in highly localized increases in ATP concentration near to Panx1 channels and T cell receptor (TCR) signaling complexes (Junker and Hoth, 2011; Quintana et al., 2007). Junger and colleagues demonstrated that these local pools of ATP are necessary for optimal ATP release via Panx1 channels in T cells and that inhibition of mitochondrial translocation results in decreased ATP efflux (Ledderose et al., 2014). Given the T cell lineage of the Jurkat leukemia cells, we considered the possibility that mitochondria might also localize at the plasma membrane during apoptosis to support Panx1-mediated ATP efflux and that FADD deficiency might disrupt this localization to decrease release of adenine nucleotides. We used MitoTracker® Red to visualize mitochondrial localization in WT and FADD-deficient Jurkat cells before and after STS treatment for 4 hours (Fig. 3E). DAPI staining verified that the nucleus occupies much of the cytoplasmic volume in both cell lines prior to apoptotic induction and that mitochondria are localized to

the thin shell of cytosol between the nucleus and plasma membrane. STS induced equivalent nuclear fragmentation in the WT and FADD-deficient cells to result in similar diffusion of mitochondria into the expanded cytosolic volume. While these data neither rule out nor demonstrate a role for subcellular mitochondrial localization in supporting Panx1-mediated ATP efflux from apoptotic Jurkat cells, there is no indication that FADD deficiency significantly alters mitochondrial distribution.

CD73 ecto-5'-nucleotidase is upregulated in FADD-deficient Jurkat cells to rapidly metabolize AMP released during apoptosis or necroptosis

We next tested whether the decreased ATP+ADP+AMP accumulation by apoptotic FADD-deficient Jurkat cells was due to increased extracellular breakdown of adenine nucleotides released via active Panx 1 channels. The most widely studied ectonucleotidases (Table 1) are the CD39-family proteins which break down ATP and ADP to AMP and CD73 which hydrolyzes AMP to adenosine (Picher et al., 2003; Resta et al., 1998; Robson et al., 2006; Stagg and Smyth, 2010; Yegutkin, 2008). While both CD39 and CD73 can be upregulated in certain types of cancers, CD73, in particular, has been linked to chemotherapy-resistant cancers and high CD73 levels are an indicator of poor prognosis (Antonioli et al., 2013b; Dzhandzhugazyan et al., 1998; Loi et al., 2013; Nevedomskaya et al., 2016; Stagg et al., 2011; Stagg and Smyth, 2010; Young et al., 2014). As noted previously, we routinely measured the summed accumulation of extracellular ATP, ADP, and AMP by apoptotic cells because the progressive decline in the intracellular ATP/ AMP ratio results in greatly increased efflux of AMP, rather than ATP, via activated Panx1 channels as cells transition from early to later phases of the apoptotic cascade. Indeed, comparison of the magnitudes of the summed extracellular [ATP+ADP+AMP] (Fig 4A-i; replotted data from Figs. 2E-i and F-i) versus [ATP] alone (Fig. 4A-ii) during STS treatment of WT Jurkat cells demonstrates ATP constitutes only a few percent of total adenine nucleotide release. However, similar accumulation of extracellular ATP was observed during the first 4 h of STS in both WT and FADD-def cells which contrasted with the ~10-fold difference in extracellular [ATP+ADP+AMP] at

these time points. These data suggest that Panx1-mediated ATP and AMP efflux are similar in both cell lines but that the AMP is rapidly cleared from the extracellular compartment.

Similar comparisons of ATP+ADP+AMP (Fig. 4B-i) versus ATP (Fig. 4B-ii) accumulation in WT and FADD-deficient cells during the slower apoptotic progression induced by Etop revealed a different pattern of extracellular nucleotide dynamics. Etop induced similar time courses of ATP and ATP+ADP+AMP accumulation in the WT cells (near-linear increases with time after an initial 4 h lag period), but almost no accumulation above basal levels of either ATP or ATP+ADP+AMP in the FADD-deficient cells. This suggests both ATP and AMP can be efficiently cleared from the extracellular compartment of the FADD-deficient cells due to the slower rates of Panx1-mediated ATP and AMP efflux triggered by Etop- versus STS-induced apoptotic execution.

T cells can dynamically up- or down-regulate expression of various ecto-nucleotidases, including CD73, depending on their differentiation, polarization, or activation state (Antonioli et al., 2013b; Bono et al., 2015; Deaglio et al., 2007). Previous studies have shown that WT Jurkat T cells express very low CD39 and CD73 activity (Yegutkin et al., 2002) but that multidrug resistant clonal variants of Jurkat cells, selected for suppressed Fas expression, have increased CD73 expression (Mikhailov et al., 2008). Given that: 1) AMP is the predominant nucleotide released via Panx1 channels in apoptotic Jurkat cells (and other cell types (Yamaguchi et al., 2014)); and 2) CD73 can be dynamically up- or down-regulated during polarization and activation of normal T lymphocytes, we hypothesized that FADD-deficiency resulted in an increased CD73 activity to efficiently hydrolyze released AMP to adenosine (Fig. 4C). Comparative qPCR analysis revealed that CD73 mRNA levels were ~5-fold greater in the FADD-deficient cells relative to WT Jurkat cells (Fig. 4E). We compared the abilities of FADD-deficient versus WT Jurkat cells to hydrolyze a 1 μM pulse of exogenous AMP over a 30 min test period in the absence or presence of α,β-methylene-adenosine 5'-diphosphate (APCP). The latter is a well-characterized inhibitor of CD73 activity (Bhattarai et al., 2015; Resta et al., 1998). The WT cells hydrolyzed less than 15% of the added AMP in 30 min while the FADD-deficient cells cleared 40% of the AMP and this accelerated breakdown was suppressed by APCP (Fig. 4F).

We then compared the magnitudes of ATP+ADP+AMP accumulation by WT and FADD-deficient Jurkat cells during 4 h STS treatment in the absence or presence of APCP. The presence of 50μM APCP markedly increased (by 5-fold) ATP+ADP+AMP accumulation in the STS-stimulated FADD-deficient cells; this level of extracellular summed adenine nucleotide was similar to that in STS-treated WT cells in the absence of APCP (Fig. 4G). Similar potentiation of extracellular adenine nucleotide accumulation by APCP was observed in FADD-deficient cells treated with Etop for 12 h (data not shown). The ability of APCP to increase [ATP+ADP+AMP] was not observed when the FADD-deficient cells were cotreated with STS and zVAD (not shown); this consistent with AMP being released via caspase-3-gated Panx1 channels.

Comparison of ATP+ADP+AMP (Fig. 4C-i) versus ATP (Fig. 4C-ii) accumulation during TNFα plus BV6-induced apoptosis in WT cells versus TNFα plus BV6-induced necroptosis in FADD-deficient cells yielded additional extracellular nucleotide kinetic profiles. The kinetics and magnitudes of ATP+ADP+AMP accumulation during TNFα plus BV6-induced extrinsic apoptosis (Fig. 4C-i) in WT cells were very similar (4 h lag phase followed by steady increase over the next 8 h) to those measured during Etop-induced intrinsic apoptosis of WT cells (Fig. 4B-i). Likewise, the kinetics of ATP release from apoptotic WT cells in response to TNFα plus BV6 (Fig. C-ii) or Etop (Fig. B-ii) were similar. In contrast, necroptosis in the FADD-deficient cells rapidly triggered a 15-fold in ATP accumulation that peaked at 4 h and then declined (Fig. 4C-ii), while the ATP+ADP+AMP accumulation continued to increase until 8h (Fig. 4C-i). This robust accumulation of extracellular adenine nucleotides (Figs. 4C-i; 4C-ii) during TNFα plus BV6-induced necroptosis of the FADD-deficient cells contrasted with the near-complete absence of adenine nucleotide accumulation (Figs. 4B-i and B-ii) during Etop-induced apoptosis in same FADD-deficient background. Thus, markedly different profiles of extracellular nucleotide accumulation can occur in a given cancer cell lineage depending on the modes of regulated cell death. Notably, APCP modestly increased the ATP+ADP+AMP accumulated by TNF plus BV6-treated FADD-

deficient Jurkat cells (data not shown); this indicates that upregulated CD73 also enhances extracellular AMP→adenosine conversion during necroptosis.

Apoptotic signaling and Panx1 channel activation in RIP1-deficient Jurkat cancer cells are also uncoupled from accumulation of extracellular adenine nucleotides

RIP1 plays a central role in directing TNF/TRAIL-family receptor signaling along the cell survival, extrinsic apoptotic, or necroptotic pathways (Fig. 1A). However, RIP1/FADD/caspase-8 ripoptosome complexes can also assemble during intrinsic apoptosis triggered by chemotherapeutic drugs (Tenev et al., 2011). Given the striking phenotypic effects of FADD-deletion on modulating extracellular adenine nucleotide accumulation driven by pro-apoptotic chemotherapeutic drugs, we tested whether deficiency in RIP1, as another ripoptosome component, results in a similar phenotype. We induced extrinsic or intrinsic apoptosis in RIP1-deficient Jurkat cells (and WT cells as matched controls) with anti-Fas for 4 h, STS for 4 h or Etop for 12 h, respectively. RIP1-deficient Jurkat cells were characterized by the complete absence of detectable ATP+ADP+AMP accumulation in the extracellular medium during apoptotic induction by STS (Fig. 5A), Etop (Fig. 5B), or anti-Fas (Fig 5C). Western blot analysis indicated identical caspase-3-mediated processing of both Panx1 and PARP in the WT and RIP1-deficient cells treated with STS or Etop (Fig. 5D). Similar to the FADD-deficient cells (Fig. 3E), there was no obvious alteration in mitochondrial localization in RIP1-deficient Jurkat cells before or after apoptotic induction with STS (Fig. 5E). Likewise, analysis of YO-PRO^{2+} dye influx (Figs. 5F and 5G) or calcein^{4-} efflux (Fig. 5H) revealed similarly robust Panx1 channel functional activity in both the WT and RIP1-deficient cells during apoptotic progression.

Ecto-AMPase activity, but not CD73 expression, is increased in RIP1-deficient Jurkat cells

Given the similar phenotypes of the RIP1-deficient and FADD-deficient Jurkat cells, we tested whether the APCP inhibitor of CD73 would also rescue the ability of STS to induce accumulation of extracellular ATP+ADP+AMP in the RIP1-deficient cells. Surprisingly, inclusion of 50 μM APCP

during the STS treatment did not facilitate increased ATP+ADP+AMP accumulation in these Jurkat cells in contrast to its effects in the FADD-deficient line (Fig. 6A). We then used the same ecto-AMPase assay described for Fig.4F to compare the abilities of the WT and RIP1-deficient cells (at identical cytocrits of 2 x 10^6 cells/ml) to metabolize an exogenous pulse of 1μM AMP in the absence or presence of 50 μM APCP (Fig. 6B). The RIP1-deficient cells completely hydrolyzed this exogenous AMP within 30 min even in the presence of APCP; this contrasted with the respective 10-20% AMP clearance activities (inhibitable by APCP) of the WT cells. Notably, qPCR analysis revealed 10-fold lower levels of CD73 mRNA in these cells relative to WT Jurkat cells (Fig. 6C). This contrasted with the 5-fold higher (relative to WT) levels of CD73 mRNA in the FADD-deficient cells (Fig. 4E). Taken together, these findings indicate that RIP1-deficient Jurkat cells upregulate ectoenzymes other than CD73 for robust clearance of the extracellular AMP released during intrinsic or extrinsic apoptosis.

Increased ecto-AMPase activity in RIP1-deficient Jurkat cells correlates with upregulation of prostatic acid phosphatase (PAP)

Three additional ectoenzymes that can metabolize extracellular AMP are AMP deaminase, tissue non-selective alkaline phosphatase (TNAP) and prostatic acid phosphatase (PAP) (Fig. 7A and Table 1). AMP deaminase (AMPD), which has been described in extracellular neuromuscular synaptic junctions (Magalhaes-Cardoso et al., 2003), catalyzes conversion of AMP to IMP, is distinct from adenosine deaminase, and can be inhibited by pentostatin/deoxycoformycin (Fishbein et al., 1981; Matsumoto et al., 1979; Zabielska et al., 2015). TNAP acts as a potent ecto-AMPase in some tissues and be inhibited by levamisole or tetramisole (Millan, 2006; Picher et al., 2003). A transmembrane variant of prostatic acid phosphatase can also function as an ectonucleotidase sensitive to inhibition by L-tartrate (Araujo and Vihko, 2013; Quintero et al., 2007; Zylka et al., 2008). Extracellular adenosine may be further metabolized to inosine by adenosine deaminase, and both adenosine and inosine may be transported into cells via multiple nucleoside transporters.

We used reversed-phase HPLC to compare the metabolic fate of exogenous AMP (100 μM) added to control wildtype versus RIP-deficient Jurkat cells (Fig. 7B-i). Consistent with their low ecto-AMPase activity (Figs. 4F and 6B), control Jurkat cells converted little of the added AMP to adenosine during the 30 min test incubation. Although the RIP1-deficient cells catabolized most of the added AMP, no accumulation of IMP or adenosine and only a minor increase in inosine were observed. Inclusion of dipyridamole, which broadly inhibits most nucleoside transporters, did not increase accumulation of extracellular adenosine by the AMP-treated control Jurkat cells but slightly increased extracellular inosine (Fig. 7B-ii). In contrast, dipyridamole greatly increased accumulation of inosine and modestly elevated adenosine during hydrolysis of the added AMP by RIP1-deficient Jurkat cells. This ability of the RIP1-deficient cells to rapidly metabolize extracellular AMP to inosine might occur by either of two coupled reactions: 1) hydrolysis of AMP to adenosine followed by deamination of adenosine to inosine; or 2) deamination of AMP to IMP followed by hydrolysis of IMP to inosine (Fig. 7A).

The absence of any intermediate IMP accumulation (Fig. 7B-i) during AMP clearance by the RIP1-deficient cells argued against primary AMP deamination. However, generated IMP might also be rapidly hydrolyzed by a co-expressed ectonucleotidase. We attempted to test whether pentostatin would attenuate AMP→inosine conversion via the AMP deamination pathway, but elution of pentostatin (which is a nucleoside analog) broadly overlapped with IMP and AMP in the employed HPLC protocol. However, using the enzyme-based AMP assay we were unable to observe a suppressive effect of pentostatin on the rapid clearance of exogenously added AMP by the RIP1-deficient Jurkat cells (data not shown). Pentostatin also failed to facilitate increased accumulation of extracellular ATP+ADP+AMP during STS-induced apoptosis of the RIP1-deficient cells (Fig. 7C). Taken together, these results argue against a major role for an ecto-adenosine deaminase in this mutant Jurkat cell line. Interestingly, pentostatin modestly increased the extracellular ATP+ADP+AMP accumulation by STS-treated wildtype Jurkat cells (Fig. 7C). This may reflect increased availability of intracellular AMP – for efflux via Panx1 – due to suppression of intracellular AMP deaminase by pentostatin that is readily accumulated via nucleoside transporters.

The TNAP inhibitor tetramisole did not prevent the rapid AMP clearance by RIP1-deficient Jurkat cells (data not shown). Likewise, inclusion of tetramisole during STS-induced apoptosis of these cells failed to rescue extracellular accumulation of ATP+ADP+AMP (data not shown). Thus, increased TNAP expression does not underlie the robust ecto-AMPase activity of the RIP1-deficient cells.

To offset the complication of the three coupled reactions (AMP hydrolysis, adenosine deamination, inosine uptake) in the RIP1-deficient Jurkat line, we incubated these cells (and wildtype Jurkat cells as a control) with 10 μM ε-AMP and measured both its decrease and the corresponding increase in ε-adenosine (ε-ADO) by anion exchange HPLC and fluorescence detection (Fig. 8A). Etheno-modification of the adenine moiety on AMP or adenosine prevents their utilization by deaminases, but not by CD73 or other ecto-AMPases (Bonitati et al., 1993; Jamal et al., 1988). Additionally, ε-ADO is a poor substrate for nucleoside transporters. Fig. 8A demonstrates that ecto-ε-AMPase activity in RIP1-deficient Jurkat cells is 8- to 10-fold higher than in the WT line; it is also 4- to 5- fold greater than in the FADD-deficient line (data not shown). Consistent with the enzyme-based assay of extracellular AMP clearance, tetramisole did not suppress the robust ε-AMP → ε-ADO conversion by the RIP1-deficient cells while APCP only modestly decreased this reaction (data not shown).

Prostatic acid phosphatase, encoded by the *ACPP* gene, is a canonical marker of human prostate cancer (Araujo and Vihko, 2013). Multiple *ACPP* splice variants yield a secreted PAP isoform and another with a transmembrane anchor (TM-PAP). Recent studies have indicated that TM-PAP mRNA and enzyme activity is expressed in normal murine and human lymphoid tissues and different T cell subsets (Quintero et al., 2007; Yegutkin et al., 2014). Notably, inclusion of 10 mM L-tartrate, as a low affinity but high efficacy inhibitor of prostatic acid phosphatase isozymes, markedly (~80%) attenuated the robust ε-AMP → ε-ADO metabolism by the RIP1-deficient Jurkat cells (Fig. 8B). Although short-term treatment of intact cells with L-tartrate can be used to assess the contribution of TM-PAP to hydrolysis of exogenously added AMP or ε-AMP, prolonged treatment is cytotoxic. Thus, we were unable to test whether L-tartrate might rescue extracellular ATP+ADP+AMP accumulation during STS-induced apoptosis of RIP1-deficient Jurkat cells. However, we assessed the ability of these cells, as well

as the wildtype and FADD-deficient Jurkat cells, to hydrolyze extracellular *p*-nitrophenyl phosphate (as a non-nucleotide substrate of PAP enzymes) under physiological (pH 7.5) or acidotic (pH 6.5) conditions (Fig. 8C). Hydrolysis of *p*-nitrophenyl phosphate by RIP1-deficient Jurkat cells was ~8-fold higher than in the wildtype or FADD-deficient Jurkat cells at either pH 7.5 or 6.5. Importantly, this phosphatase activity was markedly inhibited by L-tartrate (Fig. 8C) but not the APCP inhibitor of CD73 (data not shown). Interestingly, western blot analysis with an antibody that recognizes both the secreted and transmembrane forms of PAP revealed an immunoreactive band (~70 kDa) in whole cell lysates from both RIP1-deficient and WT Jurkat cells, albeit with stronger intensity in the RIP1-deficient cells. Because TM-PAP has a lysosomal sorting signal, it can traffic to both the lysosomal and plasma membrane compartments. The large difference in ecto-phosphatase activity between the control and RIP1-deficient cells suggests that TM-PAP may be retained in lysosomes of control Jurkat cells while predominantly trafficking to the surface membrane of the RIP1-deficient cells. Taken together, these observations suggest that the membrane-anchored variant of PAP is markedly upregulated in RIP-deficient Jurkat cells to function as the robust ecto-AMPase activity that defines these leukemic T cells.

As noted previously, the initial phases of STS-stimulated extracellular ATP accumulation (Fig. 4A-ii) were similar in the WT and FADD-deficient Jurkat cells despite marked differences in total ATP+ADP+AMP accumulation (Fig.4A-i). We compared STS-stimulated extracellular ATP accumulation in WT, FADD-deficient, and RIP-deficient Jurkat cells and observed markedly reduced extracellular ATP accumulation in the RIP-deficient cells relative to the other two Jurkat lines (Fig. 8D). This is consistent with the reported ability of TM-PAP to directly metabolize ATP in addition to AMP (Table 1). Because CD39 expression is very low in WT Jurkat cells (Boyd-Tressler et al., 2014; Chekeni et al., 2010; Yegutkin et al., 2006), we also compared ecto-ATPase activity levels in WT versus RIP-deficient Jurkat cells incubated with 1 μM exogenous ATP for 30 min in the absence or presence of the CD39 inhibitor ARL67156 (ARL). While WT cells hydrolyzed only 5% of the ATP, the RIP1-deficient cells cleared ~45% of the ATP and this was partially inhibited (by ~50%) by ARL (data not shown).

Thus, increased TM-PAP and CD39 activity in RIP1-deficient Jurkat cells likely contribute to their decreased ability to accumulate extracellular ATP during STS-induced apoptosis (Fig. 8D).

Discussion

This study provides new insights regarding mechanisms of adenine nucleotide release and extracellular metabolism by cancer cells (Jurkat human leukemic T cells) during different modes of regulated cell death. First, we extended previous findings (Boyd-Tressler et al., 2014; Chekeni et al., 2010) verifying the critical role of caspase-3-activated Panx1 channels as an ATP/AMP efflux pathway to cells undergoing extrinsic apoptosis in response to the TNFR1 member of the Fas/TNFR/TRAIL death receptor family. Second, we demonstrated that redirection of TNFR1 signaling from apoptosis to necroptosis results in redirection of the ATP efflux mechanism from open-gating of Panx1 channels to insertion of RIP3-phosphorylated MLKL pores into the plasma membrane. Third, we observed that, due to its rapid *intracellular* production during both apoptotic and necroptotic progression, AMP becomes a major nucleotide substrate for both Panx1 channels and MLKL pores, resulting in its robust *extracellular* accumulation during both modes of regulated cell death. Finally, we found that genetic ablation of FADD and RIP1, two critical adapter proteins for TNFR/TRAIL death receptor signaling, uncouples caspase-3-activated Panx 1 channels from extracellular adenine nucleotide accumulation due to up-regulated expression of diverse ectonucleotidases. These included the CD73 ecto-AMPase in FADD-deficient Jurkat cells versus a membrane-anchored prostatic acid phosphatase (TM-PAP) ecto-AMPase in the RIP1-deficient Jurkat cells. This provides insight into how regulation of extracellular ATP, AMP and adenosine levels may vary during expansion of clonal variants of a given cancer cell type.

TNFR1 can signal through different cell pathways in cancer cells (Fig. 1A). TNFR1 activation of BV6-treated WT Jurkat cells induced an increase in extracellular adenine nucleotides over 12 h (after an initial 2-h lag phase). This accumulation was mediated by active Panx1 channels in the absence of overt cell lysis. These responses to TNFα recapitulated those elicited by Fas activation, but with slower kinetics. Notably, adenine nucleotide release in response to TNFα/BV6 was completely redirected from a Panx1 channels to a MLKL pores in Jurkat cells lacking expression of FADD. Other studies have described the release of ATP during necroptotic progression in human THP-1 monocytic leukemia cells

(Wang et al., 2015) and a human bronchial epithelial cell line (Pouwels et al., 2016). These reports noted that conditioned media from the necroptotic cells stimulated the P2Y receptor-mediated migration of phagocytic leukocytes similar to earlier studies using conditioned medium from apoptotic Jurkat cells (Chekeni et al., 2010; Elliott et al., 2009). Our studies support a model whereby released ATP acts as a major "find-me" signal for phagocytic leukocytes to migrate towards either apoptotic or necroptotic tumor cells as a prelude to tumor cell clearance and processing of tumor antigens for presentation to T cells.

Most studies of nucleotide release from dying cancer cells focus on extracellular accumulation of ATP given its roles as a find-me ligand for directed migration of phagocytes and a pro-immunogenic mediator (Chekeni et al., 2010; Elliott et al., 2009; Ghiringhelli et al., 2009; Ma et al., 2013; Martins et al., 2009; Martins et al., 2014; Michaud et al., 2011). However, both Panx1 channels (Chiu et al., 2014) and MLKL pores (Dondelinger et al., 2014; Galluzzi et al., 2014; Su et al., 2014) are defined by broad permeability to organic/inorganic anions and cations with molecular masses in the 1000 Da range or greater. These will include nucleotides other than ATP, such as UTP, which also acts as a find-me ligand (Chekeni et al., 2010; Lazarowski, 2012), and intracellular metabolites of ATP, such as AMP (Boyd-Tressler et al., 2014; Yamaguchi et al., 2014). Our study extends previous findings that AMP becomes the predominant nucleotide released via Panx1 channels during the progression of apoptotic execution. AMP, in addition to ATP, was also increasingly released via MLKL pores during necroptotic progressiion in TNFα/BV6-stimulated FADD-deficient Jurkat cells. Earlier studies determined that the intracellular nucleotide pool of apoptotic cells shifts from an initially high [ATP] to progressively lower [ATP] as a consequence of increased ATP utilization and decreased mitochondrial ATP synthesis (Ricci et al., 2004; Waterhouse et al., 2001). This was linked to the caspase-3-mediated cleavage and inactivation of the p75 subunit of complex I of the electron transport chain (Ricci et al., 2004). A decrease in the cytosolic [ATP]/[AMP] ratio likely also occurs during necroptosis. Using TNFα/BV6 stimulated-FADD-deficient Jurkat cells, Schenk and Fulda observed that necroptotic progression is faciliated by a positive feed-back

loop whereby activated MLKL promotes accumulation of mitochondrial reactive oxygen species (ROS) which, in turn, further stabilize formation of RIP1/RIP3 necrosomes (Schenk and Fulda, 2015). Such diversion of mitochondrial function to ROS production will decrease ATP production, while insertion of MLKL pores into the plasma will increase ATP breakdown to ADP and AMP as a result of increased Na^+, K^+-ATPase and Ca^{2+}-ATPase activity secondary to enhanced Na^+ influx (Chen et al., 2014) and Ca^{2+} influx (Cai et al., 2014) mediated by MLKL pores.

An increasing accumulation of AMP in the in vivo extracellular microenvironment of apoptotic or necroptotic tumor cells is significant due to its modulatory effects on pro-immunogenic and pro-inflammatory signaling. In contrast to ATP, AMP is not an agonistic ligand for the immunostimulatory P2 receptors expressed on phagocytic leukocytes or tumor antigen-reactive T cells. Rather, extracellular AMP is a potential source for the production of adenosine which activates the immunosuppressive A2a/ A2b adenosine receptors expressed on those leukocytes and T cells. This potential capacity of extracellular AMP to drive local accumulation of immunosuppressive adenosine will be determined by the relative expression of various ecto-AMPases on the tumor cells *per se*, adjacent stromal cells, and recruited leukocytes.

Altered expression or mutation of pro-apoptotic or pro-necroptotic signaling proteins contributes to tumor cell resistance to chemotherapeutic agents. We verified efficient intrinsic apoptosis in FADD- or RIP1-deficient Jurkat cells treated with staurosporine or etoposide, two mechanistically distinct pro-apoptotic drugs. Despite efficient gating of Panx1 channels in apoptotic FADD- or RIP1-deficient Jurkat cells, little or no extracellular adenine nucleotide accumulation was observed. This uncoupling of Panx1 channel activity from adenine nucleotide accumulation was linked to increased expression of CD73 ecto-AMPase in the FADD-deficient Jurkat line, but upregulation of TM-PAP as a robust ecto-AMPase in the RIP1-deficient Jurkat line.

Only a 2-fold increase in CD73 activity distinguished the FADD-deficient cells from the wildtype cells, but this was sufficient to markedly reduce AMP accumulation during apoptosis. The modest increase in CD73 activity also suppressed extracellular ATP accumulation in response to etoposide but

not staurosporine. This suggests that increased clearance of extracellular AMP by CD73 may relieve product inhibition of the upstream CD39 ecto-ATPase and thereby result in increased clearance of ATP if the latter is delivered to the extracellular compartment at a relatively slow rate. Indeed, the increased CD73 activity of FADD-deficient Jurkat cells was insufficient to prevent accumulation of AMP or ATP during TNFα/BV6-induced necroptosis. This implies that the rate of efflux of ATP and AMP via activated MLKL pores exceeds the rate of AMP clearance by upregulated CD73. Importantly, the CD73 inhibitor APCP rescued the apoptotic adenine nucleotide accumulation responses in the FADD-deficient cells and further enhanced necroptotic adenine nucleotide accumulation.

The absence of RIP1 expression in Jurkat cells resulted in an even more dramatic suppression of the adenine nucleotide accumulation responses during intrinsic or extrinsic apoptosis. Although the RIP1-deficient Jurkat line was characterized by a ~10-fold greater ecto-AMPase activity relative to the parental control Jurkat cell line, this was not mediated by CD73. Pharmacological approaches and HPLC-based assays of extracellular AMP metabolism ruled out contributions of tissue non-selective alkaline phosphatase and extracellular AMP deaminases. Rather, we determined that a remarkable upregulation of an L-tartrate-sensitive TM-PAP was responsible for rapid clearance of released nucleotides. Despite its canonical association with the prostate gland, recent studies have indicated that TM-PAP and/or the secreted PAP isoform function as significant ecto-nucleotidases in multiple tissues and cell types including saliva (Araujo et al., 2014), dorsal root ganglion neurons that mediate nociception (Street et al., 2011; Zylka et al., 2008), and normal T lymphocytes (Yegutkin et al., 2014). Upregulated PAP is also used as a biomarker of prostate cancer (Hakalahti et al., 1993) and our observations suggest the possibility that it may also be marker for some subtypes of leukemias. Because selective and well-defined pharmacological inhibitors of PAP ectonucleotidase activity are not readily available (Larsen et al., 2009; McCoy et al., 2013), most studies have utilized PAP-knockout mice to define physiological roles (Street et al., 2011; Yegutkin et al., 2014; Zylka et al., 2008). Studies using siRNA with Jurkat cells and other human leukemia lines would be informative to define roles for TM-PAP in the growth, survival, and immunogenicity of hematopoietic tumors.

In contrast to ATP, AMP is not an agonist for immunostimulatory P2 nucleotide receptors but is a substrate for production of immunosuppressive adenosine. Because wild-type Jurkat cells are defined by low rates of ATP and AMP hydrolysis, even modest increases in CD73 or TM-PAP altered the extracellular balance of ATP versus adenosine and may attenuate tumor immunogenicity. The mechanisms whereby altered FADD or RIP expression modulate CD73 and TM-PAP expression are unclear. However, differential expression of CD73 or TM-PAP in clonal tumor variants may determine whether chemotherapeutic drug-induced activation of Panx1 channels predominantly drive accumulation of immunostimulatory ATP versus immunosuppressive adenosine.

Acknowledgments

We thank Silva Penuela and Dale Laird (University of Western Ontario, ON Canada) for providing the anti-human pannexin-1 antisera.

Author Contributions

Participated in research design: Boyd-Tressler and Dubyak
Conducted experiments: Boyd-Tressler, Lane, and Dubyak
Performed data analysis: Boyd-Tressler and Dubyak
Wrote and reviewed manuscript: Boyd -Tressler and Dubyak

References

Antonioli L, Blandizzi C, Pacher P and Hasko G (2013a) Immunity, inflammation and cancer: a leading role for adenosine. *Nat Rev Cancer* **13**:842-857.

Antonioli L, Pacher P, Vizi ES and Hasko G (2013b) CD39 and CD73 in immunity and inflammation. *Trends in molecular medicine* **19**:355-367.

Araujo CL, Quintero IB, Kipar A, Herrala AM, Pulkka AE, Saarinen L, Hautaniemi S and Vihko P (2014) Prostatic acid phosphatase is the main acid phosphatase with 5'-ectonucleotidase activity in the male mouse saliva and regulates salivation. *American journal of physiology Cell physiology* **306**:C1017-1027.

Araujo CL and Vihko PT (2013) Structure of Acid phosphatases. *Methods in molecular biology* **1053**:155-166.

Beavis PA, Stagg J, Darcy PK and Smyth MJ (2012) CD73: a potent suppressor of antitumor immune responses. *Trends in immunology* **33**:231-237.

Belz K, Schoeneberger H, Wehner S, Weigert A, Bonig H, Klingebiel T, Fichtner I and Fulda S (2014) Smac mimetic and glucocorticoids synergize to induce apoptosis in childhood ALL by promoting ripoptosome assembly. *Blood* **124**:240-250.

Bhattarai S, Freundlieb M, Pippel J, Meyer A, Abdelrahman A, Fiene A, Lee SY, Zimmermann H, Yegutkin GG, Strater N, El-Tayeb A and Muller CE (2015) alpha,beta-Methylene-ADP (AOPCP) Derivatives and Analogues: Development of Potent and Selective ecto-5'-Nucleotidase (CD73) Inhibitors. *J Med Chem* **58**:6248-6263.

Bonitati AE, Agarwal KC and Rounds S (1993) A simple assay for ecto-5'-nucleotidase using intact pulmonary artery endothelial cells. Effect of endotoxin-induced cell injury. *Biochemical pharmacology* **46**:1467-1473.

Bono MR, Fernandez D, Flores-Santibanez F, Rosemblatt M and Sauma D (2015) CD73 and CD39 ectonucleotidases in T cell differentiation: Beyond immunosuppression. *FEBS letters* **589**:3454-3460.

Boyd-Tressler A, Penuela S, Laird DW and Dubyak GR (2014) Chemotherapeutic drugs induce ATP release via caspase-gated pannexin-1 channels and a caspase/pannexin-1-independent mechanism. *The Journal of biological chemistry* **289**:27246-27263.

Cai Z, Jitkaew S, Zhao J, Chiang HC, Choksi S, Liu J, Ward Y, Wu LG and Liu ZG (2014) Plasma membrane translocation of trimerized MLKL protein is required for TNF-induced necroptosis. *Nature cell biology* **16**:55-65.

Chekeni FB, Elliott MR, Sandilos JK, Walk SF, Kinchen JM, Lazarowski ER, Armstrong AJ, Penuela S, Laird DW, Salvesen GS, Isakson BE, Bayliss DA and Ravichandran KS (2010) Pannexin 1 channels mediate 'find-me' signal release and membrane permeability during apoptosis. *Nature* **467**:863-867.

Chen X, Li W, Ren J, Huang D, He WT, Song Y, Yang C, Li W, Zheng X, Chen P and Han J (2014) Translocation of mixed lineage kinase domain-like protein to plasma membrane leads to necrotic cell death. *Cell research* **24**:105-121.

Chiu YH, Ravichandran KS and Bayliss DA (2014) Intrinsic properties and regulation of Pannexin 1 channel. *Channels* **8**:103-109.

Deaglio S, Dwyer KM, Gao W, Friedman D, Usheva A, Erat A, Chen JF, Enjyoji K, Linden J, Oukka M, Kuchroo VK, Strom TB and Robson SC (2007) Adenosine generation catalyzed by CD39 and CD73 expressed on regulatory T cells mediates immune suppression. *The Journal of experimental medicine* **204**:1257-1265.

Dondelinger Y, Declercq W, Montessuit S, Roelandt R, Goncalves A, Bruggeman I, Hulpiau P, Weber K, Sehon CA, Marquis RW, Bertin J, Gough PJ, Savvides S, Martinou JC, Bertrand MJ and Vandenabeele P (2014) MLKL Compromises Plasma Membrane Integrity by Binding to Phosphatidylinositol Phosphates. *Cell reports* **7**:971-981.

Dzhandzhugazyan KN, Kirkin AF, thor Straten P and Zeuthen J (1998) Ecto-ATP diphosphohydrolase/CD39 is overexpressed in differentiated human melanomas. *FEBS letters* **430**:227-230.

Elliott MR, Chekeni FB, Trampont PC, Lazarowski ER, Kadl A, Walk SF, Park D, Woodson RI, Ostankovich M, Sharma P, Lysiak JJ, Harden TK, Leitinger N and Ravichandran KS (2009) Nucleotides released by apoptotic cells act as a find-me signal to promote phagocytic clearance. *Nature* **461**:282-286.

Feoktistova M, Geserick P, Kellert B, Dimitrova DP, Langlais C, Hupe M, Cain K, MacFarlane M, Hacker G and Leverkus M (2011) cIAPs block Ripoptosome formation, a RIP1/caspase-8 containing intracellular cell death complex differentially regulated by cFLIP isoforms. *Molecular cell* **43**:449-463.

Fishbein WN, Davis JI, Winkert JW and Strong DM (1981) Levels of adenosine deaminase AMP deaminase, and adenylate kinase in cultured human lymphoblast lines: exquisite sensitivity of AMP deaminase to adenosine deaminase inhibitors. *Biochem Med* **26**:377-386.

Galluzzi L, Kepp O and Kroemer G (2014) MLKL regulates necrotic plasma membrane permeabilization. *Cell research* **24**:139-140.

Ghiringhelli F, Apetoh L, Tesniere A, Aymeric L, Ma Y, Ortiz C, Vermaelen K, Panaretakis T, Mignot G, Ullrich E, Perfettini JL, Schlemmer F, Tasdemir E, Uhl M, Genin P, Civas A, Ryffel B, Kanellopoulos J, Tschopp J, Andre F, Lidereau R, McLaughlin NM, Haynes NM, Smyth MJ, Kroemer G and Zitvogel L (2009) Activation of the NLRP3 inflammasome in dendritic cells induces IL-1beta-dependent adaptive immunity against tumors. *Nature medicine* **15**:1170-1178.

Gude DR, Alvarez SE, Paugh SW, Mitra P, Yu J, Griffiths R, Barbour SE, Milstien S and Spiegel S (2008) Apoptosis induces expression of sphingosine kinase 1 to release sphingosine-1-phosphate as a "come-and-get-me" signal. *FASEB journal : official publication of the Federation of American Societies for Experimental Biology* **22**:2629-2638.

Hakalahti L, Vihko P, Henttu P, Autio-Harmainen H, Soini Y and Vihko R (1993) Evaluation of PAP and PSA gene expression in prostatic hyperplasia and prostatic carcinoma using northern-blot analyses, in situ hybridization and immunohistochemical stainings with monoclonal and bispecific antibodies. *Int J Cancer* **55**:590-597.

Hampp R (1985) Luminometric Method, in *Methods of Enzymatic Analysis* (Bergmeyer HU ed) p 370, Verlag Chemie, Weinheim.

Humphries F, Yang S, Wang B and Moynagh PN (2015) RIP kinases: key decision makers in cell death and innate immunity. *Cell death and differentiation* **22**:225-236.

Jamal Z, Afkham-Ebrahimi A and Saggerson ED (1988) A novel assay for 5'-nucleotidase using 1,N6-etheno-AMP as substrate, and comments on the properties of the reaction product, ethenoadenosine. *The Biochemical journal* **250**:369-373.

Junker C and Hoth M (2011) Immune synapses: mitochondrial morphology matters. *The EMBO journal* **30**:1187-1189.

Kepp O, Tesniere A, Zitvogel L and Kroemer G (2009) The immunogenicity of tumor cell death. *Curr Opin Oncol* **21**:71-76.

Larsen RS, Zylka MJ and Scott JE (2009) A high throughput assay to identify small molecule modulators of prostatic acid phosphatase. *Curr Chem Genomics* **3**:42-49.

Lazarowski ER (2012) Vesicular and conductive mechanisms of nucleotide release. *Purinergic signalling* **8**:359-373.

Ledderose C, Bao Y, Lidicky M, Zipperle J, Li L, Strasser K, Shapiro NI and Junger WG (2014) Mitochondria are gate-keepers of T cell function by producing the ATP that drives purinergic signaling. *The Journal of biological chemistry* **289**:25936-25945.

Loi S, Pommey S, Haibe-Kains B, Beavis PA, Darcy PK, Smyth MJ and Stagg J (2013) CD73 promotes anthracycline resistance and poor prognosis in triple negative breast cancer. *Proceedings of the National Academy of Sciences of the United States of America* **110**:11091-11096.

Ma Y, Adjemian S, Yang H, Catani JP, Hannani D, Martins I, Michaud M, Kepp O, Sukkurwala AQ, Vacchelli E, Galluzzi L, Zitvogel L and Kroemer G (2013) ATP-dependent recruitment, survival and differentiation of dendritic cell precursors in the tumor bed after anticancer chemotherapy. *Oncoimmunology* **2**:e24568.

Magalhaes-Cardoso MT, Pereira MF, Oliveira L, Ribeiro JA, Cunha RA and Correia-de-Sa P (2003) Ecto-AMP deaminase blunts the ATP-derived adenosine A2A receptor facilitation of acetylcholine release at rat motor nerve endings. *The Journal of physiology* **549**:399-408.

Martinou JC and Youle RJ (2011) Mitochondria in apoptosis: Bcl-2 family members and mitochondrial dynamics. *Developmental cell* **21**:92-101.

Martins I, Tesniere A, Kepp O, Michaud M, Schlemmer F, Senovilla L, Seror C, Metivier D, Perfettini JL, Zitvogel L and Kroemer G (2009) Chemotherapy induces ATP release from tumor cells. *Cell cycle* **8**:3723-3728.

Martins I, Wang Y, Michaud M, Ma Y, Sukkurwala AQ, Shen S, Kepp O, Metivier D, Galluzzi L, Perfettini JL, Zitvogel L and Kroemer G (2014) Molecular mechanisms of ATP secretion during immunogenic cell death. *Cell death and differentiation* **21**:79-91.

Matsumoto SS, Raivio KO and Seegmiller JE (1979) Adenine nucleotide degradation during energy depletion in human lymphoblasts. Adenosine accumulation and adenylate energy charge correlation. *The Journal of biological chemistry* **254**:8956-8962.

McCoy ES, Lea WA, Mott BT, Maloney DJ, Jadhav A, Simeonov A and Zylka MJ (2013) High-throughput screen identifies cyclic nucleotide analogs that inhibit prostatic acid phosphatase. *J Biomol Screen* **18**:481-489.

Michaud M, Martins I, Sukkurwala AQ, Adjemian S, Ma Y, Pellegatti P, Shen S, Kepp O, Scoazec M, Mignot G, Rello-Varona S, Tailler M, Menger L, Vacchelli E, Galluzzi L, Ghiringhelli F, di Virgilio F, Zitvogel L and Kroemer G (2011) Autophagy-dependent anticancer immune responses induced by chemotherapeutic agents in mice. *Science* **334**:1573-1577.

Mikhailov A, Sokolovskaya A, Yegutkin GG, Amdahl H, West A, Yagita H, Lahesmaa R, Thompson LF, Jalkanen S, Blokhin D and Eriksson JE (2008) CD73 participates in cellular multiresistance program and protects against TRAIL-induced apoptosis. *Journal of immunology* **181**:464-475.

Millan JL (2006) Alkaline Phosphatases : Structure, substrate specificity and functional relatedness to other members of a large superfamily of enzymes. *Purinergic signalling* **2**:335-341.

Morgan MJ, Kim YS and Liu ZG (2009) Membrane-bound Fas ligand requires RIP1 for efficient activation of caspase-8 within the death-inducing signaling complex. *Journal of immunology* **183**:3278-3284.

Nevedomskaya E, Perryman R, Solanki S, Syed N, Mayboroda OA and Keun HC (2016) A Systems Oncology Approach Identifies NT5E as a Key Metabolic Regulator in Tumor Cells and Modulator of Platinum Sensitivity. *Journal of proteome research* **15**:280-290.

Penuela S, Bhalla R, Gong XQ, Cowan KN, Celetti SJ, Cowan BJ, Bai D, Shao Q and Laird DW (2007) Pannexin 1 and pannexin 3 are glycoproteins that exhibit many distinct characteristics from the connexin family of gap junction proteins. *Journal of cell science* **120**:3772-3783.

Penuela S, Bhalla R, Nag K and Laird DW (2009) Glycosylation regulates pannexin intermixing and cellular localization. *Molecular biology of the cell* **20**:4313-4323.

Penuela S, Gehi R and Laird DW (2013) The biochemistry and function of pannexin channels. *Biochimica et biophysica acta* **1828**:15-22.

Peter C, Waibel M, Keppeler H, Lehmann R, Xu G, Halama A, Adamski J, Schulze-Osthoff K, Wesselborg S and Lauber K (2012) Release of lysophospholipid 'find-me' signals during apoptosis requires the ATP-binding cassette transporter A1. *Autoimmunity* **45**:568-573.

Peter C, Waibel M, Radu CG, Yang LV, Witte ON, Schulze-Osthoff K, Wesselborg S and Lauber K (2008) Migration to apoptotic "find-me" signals is mediated via the phagocyte receptor G2A. *The Journal of biological chemistry* **283**:5296-5305.

Picher M, Burch LH, Hirsh AJ, Spychala J and Boucher RC (2003) Ecto 5'-nucleotidase and nonspecific alkaline phosphatase. Two AMP-hydrolyzing ectoenzymes with distinct roles in human airways. *The Journal of biological chemistry* **278**:13468-13479.

Poon IK, Chiu YH, Armstrong AJ, Kinchen JM, Juncadella IJ, Bayliss DA and Ravichandran KS (2014) Unexpected link between an antibiotic, pannexin channels and apoptosis. *Nature* **507**:329-334.

Pouwels SD, Zijlstra GJ, van der Toorn M, Hesse L, Gras R, Ten Hacken NH, Krysko DV, Vandenabeele P, de Vries M, van Oosterhout AJ, Heijink IH and Nawijn MC (2016) Cigarette smoke-induced necroptosis and DAMP release trigger neutrophilic airway inflammation in mice. *Am J Physiol Lung Cell Mol Physiol* **310**:L377-386.

Quintana A, Schwindling C, Wenning AS, Becherer U, Rettig J, Schwarz EC and Hoth M (2007) T cell activation requires mitochondrial translocation to the immunological synapse. *Proceedings of the National Academy of Sciences of the United States of America* **104**:14418-14423.

Quintero IB, Araujo CL, Pulkka AE, Wirkkala RS, Herrala AM, Eskelinen EL, Jokitalo E, Hellstrom PA, Tuominen HJ, Hirvikoski PP and Vihko PT (2007) Prostatic acid phosphatase is not a prostate specific target. *Cancer research* **67**:6549-6554.

Resta R, Yamashita Y and Thompson LF (1998) Ecto-enzyme and signaling functions of lymphocyte CD73. *Immunological reviews* **161**:95-109.

Ricci JE, Munoz-Pinedo C, Fitzgerald P, Bailly-Maitre B, Perkins GA, Yadava N, Scheffler IE, Ellisman MH and Green DR (2004) Disruption of mitochondrial function during apoptosis is mediated by caspase cleavage of the p75 subunit of complex I of the electron transport chain. *Cell* **117**:773-786.

Robson SC, Sevigny J and Zimmermann H (2006) The E-NTPDase family of ectonucleotidases: Structure function relationships and pathophysiological significance. *Purinergic signalling* **2**:409-430.

Sandilos JK, Chiu YH, Chekeni FB, Armstrong AJ, Walk SF, Ravichandran KS and Bayliss DA (2012) Pannexin 1, an ATP release channel, is activated by caspase cleavage of its pore-associated C-terminal autoinhibitory region. *The Journal of biological chemistry* **287**:11303-11311.

Schenk B and Fulda S (2015) Reactive oxygen species regulate Smac mimetic/TNFalpha-induced necroptotic signaling and cell death. *Oncogene* **34**:5796-5806.

Stagg J, Divisekera U, Duret H, Sparwasser T, Teng MW, Darcy PK and Smyth MJ (2011) CD73-deficient mice have increased antitumor immunity and are resistant to experimental metastasis. *Cancer research* **71**:2892-2900.

Stagg J and Smyth MJ (2010) Extracellular adenosine triphosphate and adenosine in cancer. *Oncogene* **29**:5346-5358.

Street SE, Walsh PL, Sowa NA, Taylor-Blake B, Guillot TS, Vihko P, Wightman RM and Zylka MJ (2011) PAP and NT5E inhibit nociceptive neurotransmission by rapidly hydrolyzing nucleotides to adenosine. *Mol Pain* **7**:80.

Su L, Quade B, Wang H, Sun L, Wang X and Rizo J (2014) A plug release mechanism for membrane permeation by MLKL. *Structure* **22**:1489-1500.

Sun L, Wang H, Wang Z, He S, Chen S, Liao D, Wang L, Yan J, Liu W, Lei X and Wang X (2012) Mixed lineage kinase domain-like protein mediates necrosis signaling downstream of RIP3 kinase. *Cell* **148**:213-227.

Tenev T, Bianchi K, Darding M, Broemer M, Langlais C, Wallberg F, Zachariou A, Lopez J, MacFarlane M, Cain K and Meier P (2011) The Ripoptosome, a signaling platform that assembles in response to genotoxic stress and loss of IAPs. *Molecular cell* **43**:432-448.

Truman LA, Ford CA, Pasikowska M, Pound JD, Wilkinson SJ, Dumitriu IE, Melville L, Melrose LA, Ogden CA, Nibbs R, Graham G, Combadiere C and Gregory CD (2008) CX3CL1/fractalkine is released from apoptotic lymphocytes to stimulate macrophage chemotaxis. *Blood* **112**:5026-5036.

Vacchelli E, Ma Y, Baracco EE, Sistigu A, Enot DP, Pietrocola F, Yang H, Adjemian S, Chaba K, Semeraro M, Signore M, De Ninno A, Lucarini V, Peschiaroli F, Businaro L, Gerardino A, Manic G, Ulas T, Gunther P, Schultze JL, Kepp O, Stoll G, Lefebvre C, Mulot C, Castoldi F, Rusakiewicz S, Ladoire S, Apetoh L, Bravo-San Pedro JM, Lucattelli M, Delarasse C, Boige V, Ducreux M, Delaloge S, Borg C, Andre F, Schiavoni G, Vitale I, Laurent-Puig P, Mattei F, Zitvogel L and Kroemer G (2015) Chemotherapy-induced antitumor immunity requires formyl peptide receptor 1. *Science* **350**:972-978.

Wang H, Sun L, Su L, Rizo J, Liu L, Wang LF, Wang FS and Wang X (2014) Mixed lineage kinase domain-like protein MLKL causes necrotic membrane disruption upon phosphorylation by RIP3. *Molecular cell* **54**:133-146.

Wang Q, Ju X, Zhou Y and Chen K (2015) Necroptotic cells release find-me signal and are engulfed without proinflammatory cytokine production. *In Vitro Cell Dev Biol Anim* **51**:1033-1039.

Waterhouse NJ, Goldstein JC, von Ahsen O, Schuler M, Newmeyer DD and Green DR (2001) Cytochrome c maintains mitochondrial transmembrane potential and ATP generation after outer mitochondrial membrane permeabilization during the apoptotic process. *The Journal of cell biology* **153**:319-328.

Yamaguchi H, Maruyama T, Urade Y and Nagata S (2014) Immunosuppression via adenosine receptor activation by adenosine monophosphate released from apoptotic cells. *Elife* **3**:e02172.

Yegutkin GG (2008) Nucleotide- and nucleoside-converting ectoenzymes: Important modulators of purinergic signalling cascade. *Biochimica et biophysica acta* **1783**:673-694.

Yegutkin GG, Auvinen K, Karikoski M, Rantakari P, Gerke H, Elima K, Maksimow M, Quintero IB, Vihko P, Salmi M and Jalkanen S (2014) Consequences of the lack of CD73 and prostatic acid phosphatase in the lymphoid organs. *Mediators of inflammation* **2014**:485743.

Yegutkin GG, Henttinen T, Samburski SS, Spychala J and Jalkanen S (2002) The evidence for two opposite, ATP-generating and ATP-consuming, extracellular pathways on endothelial and lymphoid cells. *The Biochemical journal* **367**:121-128.

Yegutkin GG, Mikhailov A, Samburski SS and Jalkanen S (2006) The detection of micromolar pericellular ATP pool on lymphocyte surface by using lymphoid ecto-adenylate kinase as intrinsic ATP sensor. *Molecular biology of the cell* **17**:3378-3385.

Young A, Mittal D, Stagg J and Smyth MJ (2014) Targeting cancer-derived adenosine: new therapeutic approaches. *Cancer Discov* **4**:879-888.

Zabielska MA, Borkowski T, Slominska EM and Smolenski RT (2015) Inhibition of AMP deaminase as therapeutic target in cardiovascular pathology. *Pharmacol Rep* **67**:682-688.

Zitvogel L, Apetoh L, Ghiringhelli F and Kroemer G (2008) Immunological aspects of cancer chemotherapy. *Nature reviews Immunology* **8**:59-73.

Zylka MJ, Sowa NA, Taylor-Blake B, Twomey MA, Herrala A, Voikar V and Vihko P (2008) Prostatic acid phosphatase is an ectonucleotidase and suppresses pain by generating adenosine. *Neuron* **60**:111-122.

Footnotes

This research was supported by the National Institutes of Health: Institute of General Medical Sciences [R01-GM36387]; [T32-GM00803]; and National Eye Institute [R01-EY014362].

Figure Legends

<u>Figure 1:</u> TNFα-induction of necroptosis or extrinsic apoptosis induces release of adenine nucleotides from Jurkat cancer cells via mechanistically distinct pathways

A. A schematic of cell death signaling and adenine nucleotide release pathways regulated by Fas and TNF receptors. B-G. WT Jurkat cells were treated with either 250ng/mL αFas for the indicated times or were pretreated with 3μM of the Smac-mimetic BV6 for 2 h followed by stimulation with 20ng/mL TNF-α for the indicated times. FADD-deficient Jurkat cells were pretreated with 3μM BV6 for 2 h followed by stimulation with 20ng/mL TNF-α for the indicated times. Parallel samples were stimulated with death receptor ligands in the presence or absence of 20 μM zVAD or 1μM NSA as indicated. B-C. Samples of conditioned extracellular media were collected at 0h, 2h, 4h, 8h, and 12h post treatment and assayed for LDH activity. LDH released from TNFα+Smac mimetic (TS)-treated cells was assayed, analyzed and normalized to the LDH released from detergent-lysed cells, Experiments with each agent were repeated 3-4 times with data indicating mean ± S.E. for n=4 (WT) and n=3 (FADD-deficient) independent experiments. Analysis by two-way ANOVA and Tukey post-test comparison; a: TS-stimulated +zVAD versus -zVAD; b: TS-stimulated +NSA versus -NSA. D-F. Cells were treated with either αFas (D) or TS (E and F) and conditioned extracellular media samples was collected at 0h, 2h, 4h, 8h, and 12h post treatment and analyzed for summed ATP+ADP+AMP. Data indicate mean ± S.E. of n=3 independent experiments. Analysis by two-way ANOVA and Tukey post-test comparison; a: αFas- or TS-treated +zVAD versus -zVAD; b: TS-stimulated +NSA versus -NSA. G-I. Whole cell lysates were prepared at the indicated times post treatment for western blot analysis as described in the "Experimental Procedures" and probed for Panx1, PARP, and actin. Data are representative of 3 experiments for each condition. All panels: ns, not significant; **, $p< 0.01$; ***, $p< 0.001$; ****, $p< 0.0001$.

Figure 2: Intrinsic apoptotic signaling and Panx1 channel cleavage in FADD-deficient Jurkat cancer cells is uncoupled from accumulation of extracellular adenine nucleotides

WT and FADD-deficient cells were treated with 3μM STS, 20μM Etop, or 250ng/mL αFas in the presence of 100μM zVAD or 1μM NSA as indicated. A-B. Whole cell lysates were prepared at the indicated times post treatment for western blot analysis and probed for Panx1, PARP, and actin. Data are representative of 3 experiments for each cell type and condition. C-D. Conditioned extracellular media samples were collected from STS-treated WT cells (C-i), Etop-treated WT cells (C-ii), STS-treated FADD-deficient (FADD-def) cells (D-i), or Etop-treated FADD-def cells (D-ii) at 0h, 2h, 4h, 8h, and 12h post treatment and assayed for release of LDH as described in Fig 1. Data indicate mean ± S.E. n=3 independent experiments. Analysis by two-way ANOVA and Tukey post-test comparison; a: STS- or Etop-stimulated +zVAD versus -zVAD; b: STS- or Etop-stimulated +NSA versus -NSA. E and F. WT and FADD-def were treated with 3μM STS or 20μM Etop in the presence or absence of 100μM zVAD or 1μM NSA where indicated. Conditioned extracellular media samples were collected from STS-treated WT cells (E-i), Etop-treated WT cells (E-ii), STS-treated (FADD-def cells (F-i), or Etop-treated FADD-def cells (F-ii) at 0h, 2h, 4h, 8h, and 12h post treatment and assayed for total ATP+ADP+AMP as described in the "Experimental Procedures". Data indicate mean ± S.E. of n=3 independent experiments. Analysis by two-way ANOVA and Tukey post-test comparison; a: STS- or Etop-stimulated +zVAD versus -zVAD; b: STS- or Etop-stimulated +NSA versus -NSA. All panels: ns, not significant; *, $p<0.05$; **, $p< 0.01$; ***, $p< 0.001$; ****, $p< 0.0001$.

Figure 3: Caspase-3-cleaved Panx1 channels are functionally active in FADD-deficient Jurkat cancer cells during intrinsic apoptosis

A. Schematic illustrates caspase-3-mediated proteolytic activation of Panx1 channel function as a pathway for ATP release or efflux/influx of charged organic dyes. B and D: WT or FADD-deficient Jurkat cells were treated with 3μM STS for 4 h or 20μM Etop for 12h. The cells were then washed, resuspended in basal salt solution supplemented with 1μM YO-PRO^{2+}, and incubated for 20 min prior to

quantification of YO-PRO^{2+} fluorescence per well or phase-contrast/epifluorescence imaging. B. Data indicate mean ± S.E. from n=3 independent experiments. Analysis by two-way ANOVA and Tukey post-test comparison; a: +STS versus -STS; b: FADD-def versus WT. D. Images are representative of 2-3 independent experiments with each stimulus. C. WT or FADD-deficient Jurkat cells were loaded with 1μM calcein-AM and then treated with STS for 4h in the presence or absence of 100μM zVAD or 50μM Trovafloxacin (Trov). Cells were then washed and resuspended in basal salt solution and calcein fluorescence was quantified. Data indicate mean ± S.E. from n=3 independent experiments. Analysis by two-way ANOVA and Tukey post-test comparison; a: +STS versus -STS; b: FADD-def versus WT; c: +STS with zVAD or Trov versus +STS alone. E. WT or FADD-deficient Jurkat cells were treated with STS for 4hr and then stained with MitoTracker® Red and DAPI. Cells were imaged by confocal microscopy at a 60X magnification. Data are representative images of n=15-19 individual cells. All panels: ns, not significant; *, $p<0.05$; **, $p< 0.01$; ***, $p< 0.001$; ****, $p< 0.0001$.

<u>Figure 4:</u> CD73 ecto-5'-nucleotidase is upregulated in FADD-deficient Jurkat cells to rapidly metabolize AMP released during apoptosis or necroptosis

A, B, C. WT and FADD-deficient cells were treated with 3μM STS (A-i and A-ii), 20μM Etop (B-i and B-ii)), or TNFα plus BV6 Smac-mimetic (TS) (C-i and C-ii). Conditioned medium samples were collected at 0h, 2h, 4h, 8h, and 12h and assayed for either summed ATP+ADP+AMP (A-i; B-i, C-i) or ATP only (A-ii, B-ii, C-ii). Data indicate mean ± S.E. of n=3 experiments and statistical analyses (two-way ANOVA with Tukey post-test comparison) of the values of FADD-def versus WT at each time point. D. Schematic of interactions between Panx1 channel-mediated adenine nucleotide efflux and metabolism of the released nucleotides by CD39 and CD73 ectonucleotidases (APCP: α,β-methylene ADP) during extrinsic or intrinsic apoptosis. E. qPCR analysis of CD73 mRNA expression in WT and FADD-deficient cells. Signals in FADD-def were normalized to signals in WT and represent values from n=3

independent experiments; analysis by two-tailed t-test. F. 1μM exogenous AMP was added to suspensions (2 x10^6/ml) of untreated WT or FADD-deficient Jurkat cells in the presence or absence of 50μM APCP. Cell-free supernatants were collected after 30 min and analyzed for the concentration of remaining [AMP]. Data indicate mean ±S.E. of 4 independent experiments with WT cells and 3 independent experiments with FADD-def cells. Analysis by two-way ANOVA and Tukey post-test comparison; a: +APCP versus -APCP; b: FADD-def versus WT. G. WT or FADD-deficient Jurkat cells were treated with 3μM STS for 4 h in the absence or presence of 50μM APCP. Conditioned medium samples were collected and assayed for summed ATP+ADP+AMP. Data indicate mean ± S.E. of n=6 independent experiments with WT cells and n=5 independent experiments with FADD-def cells. Analysis by two-way ANOVA and Tukey post-test comparison; a: +STS versus -STS; b: FADD-def versus WT; c: +STS with APCP versus STS alone. All panels: ns, not significant; *, $p<0.05$; **, $p< 0.01$; ***, $p< 0.001$; ****, $p< 0.0001$.

<u>Figure 5:</u> Apoptotic signaling and Panx1 channel activation in RIP1-deficient Jurkat cancer cells is also uncoupled from accumulation of extracellular adenine nucleotides

A, B, C. WT and RIP1-deficient Jurkat cells were treated with 3 μM STS for 4 h (A), 20μM Etop for 12h (B), or 250ng/mL αFas for 4 h (C); conditioned extracellular media samples were collected and assayed for total ATP+ADP+AMP accumulation. Data indicate mean ± S.E. for n=3 independent experiments. Analysis by two-way ANOVA and Tukey post-test comparison; a: post-incubation ATP+ADP+AMP versus background ATP+ADP+AMP at time 0; b: RIP1-def versus WT. D. WT or RIP1-deficient cells were treated with STS or Etop as described prior to preparation of whole cell lysates for SDS-PAGE and western blot analysis of Panx1, PARP and actin. Data are representative of 3 experiments. E. WT and RIP1-deficient Jurkat cells were treated with STS for 4hr and then stained with MitoTracker® Red and DAPI. Cells were imaged by confocal microscopy at a 60X magnification. Data are representative images of n=15-19 individual cells. F. RIP1-deficient cells were treated with STS or Etop for 4 or 12

hours, respectively, and cell suspensions were analyzed for YO-PRO2+ accumulation. Representative phase-contrast and epifluorescence microscopy images from 3 experiments. G. WT and RIP1-deficient Jurkat cells were treated with 3μM STS for 4h and then washed and resuspended in basal salt solution supplemented with 1μM YO-PRO^{2+}; the cell suspensions were incubated for 20 min prior to quantification of YO-PRO fluorescence per well. Data indicate mean ± S.E. from n=3 independent experiments. Analysis by two-way ANOVA and Tukey post-test comparison; a: +STS versus -STS; b: RIP1-def versus WT. H. WT, and RIP1-deficient Jurkat cells were loaded with 1μM calcein-AM and then treated with STS for 4h in the presence or absence of 100μM zVAD or 50μM Trov. Cells were then washed and resuspended in basal salt solution and calcein^{4-} fluorescence was measured. Data indicate mean ± S.E. from n=3 independent experiments. Analysis by two-way ANOVA and Tukey post-test comparison; a: +STS versus -STS; b: RIP1-def versus WT; c: +STS with zVAD or Trov versus +STS alone. All panels: ns, not significant; *, $p<0.05$; **, $p< 0.01$; ***, $p< 0.001$; ****, $p< 0.0001$.

Figure 6: Ecto-AMPase activity, but not CD73 expression, is increased in RIP1-deficient Jurkat cells

A. WT or RIP1-deficient Jurkat cells were treated without or with STS for 4h in the presence or absence of 50μM APCP. Extracellular media samples were collected and analyzed for total ATP+ADP+AMP. Data indicate mean ± S.E. of n=6 independent experiments with WT cells and n=5 independent experiments with RIP1-def cells. Analysis by two-way ANOVA and Tukey post-test comparison; a: +STS versus -STS; b: RIP1-def versus WT; c: +STS with APCP versus STS alone. B. WT or RIP1-deficient cells were suspended at $2x10^6$/mL. 1μM exogenous AMP was added in the presence or absence of 50μM APCP and cell-free supernatants were collected after 30 min and analyzed for remaining [AMP]. Data indicate mean ±S.E. of 4 independent experiments with WT cells and 3 independent experiments with RIP1-def cells. Analysis by two-way ANOVA and Tukey post-test comparison; a: +APCP versus -APCP; b: RIP1-def versus WT. C. qPCR analysis of CD73 mRNA expression in WT and RIP1-deficient

cells. Signals in RIP1-def were normalized to signals in WT and represent values from n=3 independent experiments; analysis by two-tailed t-test. All panels: ns, not significant; ***, p< 0.001; ****, p< 0.0001.

Figure 7: Increased ecto-AMPase activity of RIP-deficient Jurkat cells is not correlated with upregulation of ecto-AMP deaminase

A. Schematic of extracellular pathways, ectoenzymes (green), and inhibitors (red) that can mediate the metabolism/clearance of released AMP. B. 100 μM AMP minus (B-i, upper traces) or plus (B-ii, lower traces) 50 μM dipyridamole was added to WT or RIP1-deficient cells ($2x10^6$ cells/mL in BSS+5mM glucose+0.1% BSA). Cell-free supernatants were collected after 30min and processed for separation and quantification of AMP, IMP, adenosine, and inosine by reverse phase HPLC and absorbance detection. Arrows indicate elution times of AMP, IMP, adenosine, and inosine standards; ? indicates an unidentified peak. Data are representative of 4-6 experiments. C. WT or RIP1-deficient Jurkat cells were treated without or with STS for 4h in the presence or absence of 50μM APCP, 200 μM pentostatin, or combined APCP plus pentostatin. Data indicate mean ±S.E. of 3 independent experiments. Analysis by two-way ANOVA and Tukey post-test comparison; a: +STS versus -STS; b:RIP1-def versus WT; c: +STS with pentostatin or pentostatin plus APCP versus STS alone. All panels: ns, not significant; *, p<0.05; **, p< 0.01; ***, p< 0.001; ****, p< 0.0001.

Figure 8: Increased ecto-AMPase activity in RIP1-deficient Jurkat cells correlates with upregulation of prostatic acid phosphatase (PAP)

A. 10μM ε-AMP was added to WT or RIP1-deficient cells ($2x10^6$ cells/mL). Cell-free supernatants were collected after 30min and processed for separation and quantification of ε-ADO and ε-AMP by anion exchange HPLC and fluorescence detection. Data are representative of 3 experiments. B. 10μM ε-AMP was added to WT or RIP1-deficient cells ($2x10^6$ cells/mL) in the absence or presence of 10 mM L-tartrate. Cell-free supernatants were collected after 30min and processed for separation and quantification

of ε-ADO and ε-AMP by anion exchange HPLC and fluorescence detection. Data are representative of 4 experiments. C. WT, RIP1-deficient, or FADD-deficient Jurkat cells (2 x10^6/ml) were plated in 96-well plates and suspended in BSS that was buffered to pH7.5 or pH 6.5. The cell suspensions were supplemented with 500 μM *p*-nitrophenyl phosphate in the absence or presence of 10 mM L-tartrate and incubated for 18 h at 25°C. Hydrolysis of nitrophenyl phosphate to nitrophenyl was assayed by measuring absorbance at 405 mm. Data indicate mean ±S.E. of 3 independent experiments. Analysis by two-way ANOVA and Tukey post-test comparison; a: + Tartrate versus -Tartrate; b:RIP1-def or FADD-def versus WT. Inset to panel C: Western blot analysis of PAP expression in whole cell lysates from WT or RIP1-deficient Jurkat cells that were resolved by SDS-PAGE and transferred to PVDF; mobility of molecular mass markers is indicated on the right. D. WT, FADD-deficient, and RIP1-deficient Jurkat cells were treated with 3μM STS for 4 hours. Extracellular media samples were collected and assayed for extracellular ATP. Data indicate mean ± S.E. of n=3 independent experiments. Analysis by two-way ANOVA and Tukey post-test comparison. All panels: ns, not significant; *, $p<0.05$; **, $p< 0.01$; ****, $p< 0.0001$.

TABLE 1: Pathways and enzymes for extracellular metabolism of nucleotides and nucleosides

Extracellular Metabolic Function	Ectoenzyme Names/ Subtypes	Catalytic Reaction	Substrate Selectivity	Inhibitors (Representative)	T cell expression
Ecto-ATPase, Ecto-ADPase, Apyrase	CD39 family; ENTDPase1-4	ATP > ADP (+Pi) > AMP (+Pi)	All purine and pyrimidine nucleotide tri/diphosphates	ARL67156; Others	Yes, but varies with differentiation and polarization state; High in Tregs
Ecto-ATP pyro-phosphatase/ phosphodisterase	ENPP1-3	ATP > AMP (+PPi)	Purine and pyrimidine nucleotide triphosphates	β,γ-methylene-ATP (competitive substrate)	Unknown but likely
Ecto-AMPase	CD73; ecto-5'-nucleotidase; (5Nte)	AMP > Ado (+Pi)	Purine and pyrimidine nucleotide monophosphates	α,β-methylene-ADP (APCP)	Yes, but varies with differentiation and polarization state; High in Tregs
Ecto-AMPase	Tissue non-selective alkaline phosphatase; (TNAP)	AMP > Ado (+Pi)	Purine and pyrimidine nucleotide monophosphates; Non-nucleotide phosphate esters	Levamisole; Tetramisole	Unknown
Ecto-AMPase, Ecto-Phosphatase	Prostatic acid phosphatase - transmembrane splice variant; (TM-PAP)	AMP (and ATP) > Ado (+Pi)	Purine and pyrimidine nucleotide phosphates; Non-nucleotide phosphate esters	L-Tartrate; Some cyclic AMP analogs	Yes, but varies with differentiation and polarization state;
Ecto-AMP Deaminase	AMPD3	AMP > IMP	AMP	Pentostatin/ deoxycoformycin	Unknown
Ecto-Adenosine Deaminase	Ecto-ADA	Ado > Ino	AMP	Pentostatin/ deoxycoformycin	Yes
Nucleoside transport (concentrative)	CNT (multiple subtypes)	Extracellular Nucleoside > Intracellular Nucleoside	All natural nucleosides; many nucleoside analogs	Dipyridimole; many others	Yes
Nucleoside transport (equilibrative)	ENT (multiple subtypes)	Extracellular Nucleoside > Intracellular Nucleoside	All natural nucleosides; many nucleoside analogs	Dipyridimole; many others	Yes

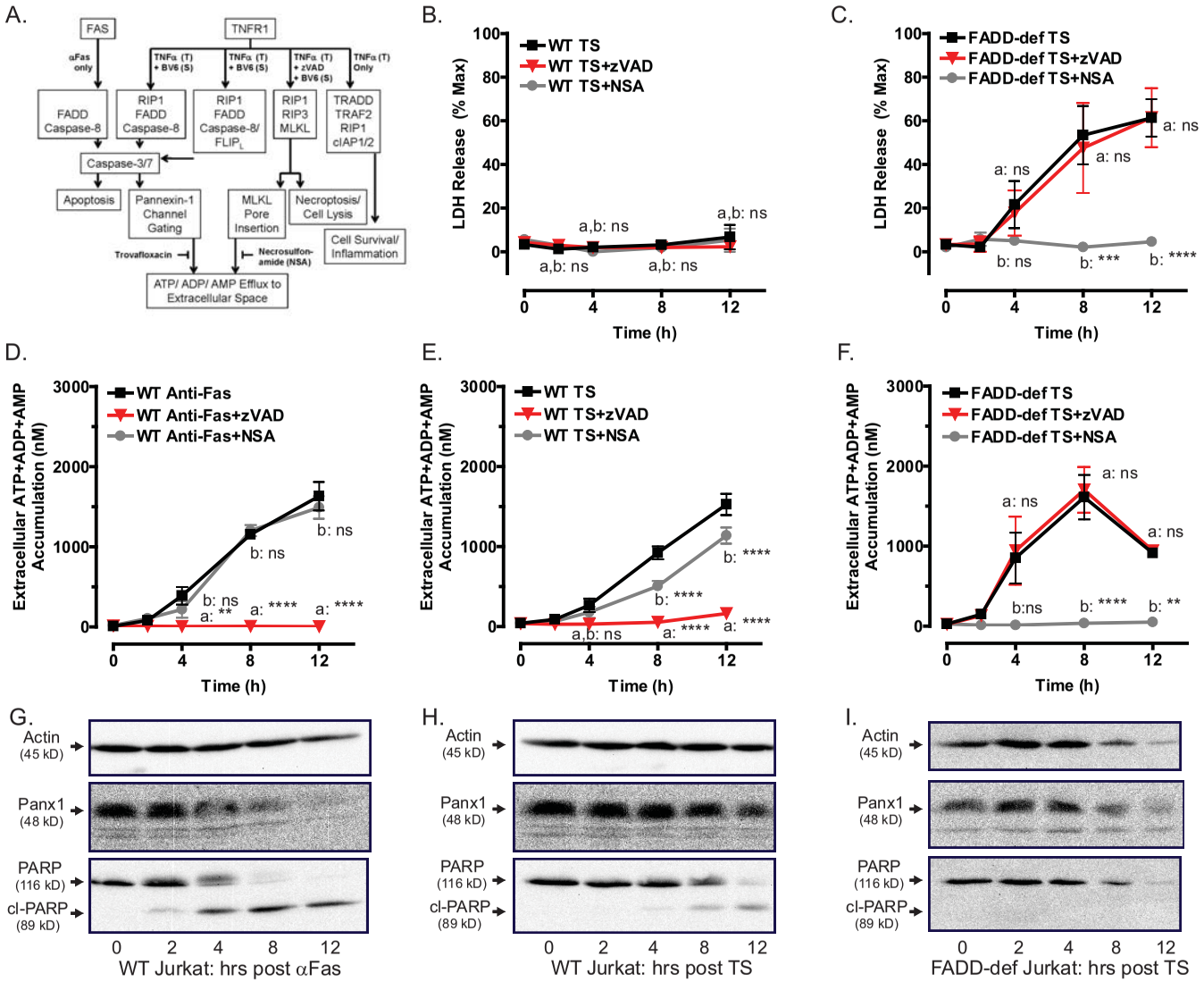
A.
FAS
TNFR1
αFas only
TNFα (T) + BV6 (S)
TNFα (T) + BV6 (S)
TNFα (T) + zVAD + BV6 (S)
TNFα (T) Only
FADD Caspase-8
RIP1 FADD Caspase-8
RIP1 FADD Caspase-8/ FLIPL
RIP1 RIP3 MLKL
TRADD TRAF2 RIP1 cIAP1/2
Caspase-3/7
Apoptosis
Pannexin-1 Channel Gating
MLKL Pore Insertion
Necroptosis/ Cell Lysis
Cell Survival/ Inflammation
Trovafloxacin
Necrosulfonamide (NSA)
ATP/ ADP/ AMP Efflux to Extracellular Space
B.
WT TS
WT TS+zVAD
WT TS+NSA
LDH Release (% Max)
Time (h)
C.
FADD-def TS
FADD-def TS+zVAD
FADD-def TS+NSA
LDH Release (% Max)
Time (h)
D.
WT Anti-Fas
WT Anti-Fas+zVAD
WT Anti-Fas+NSA
Extracellular ATP+ADP+AMP Accumulation (nM)
Time (h)
E.
WT TS
WT TS+zVAD
WT TS+NSA
Extracellular ATP+ADP+AMP Accumulation (nM)
Time (h)
F.
FADD-def TS
FADD-def TS+zVAD
FADD-def TS+NSA
Extracellular ATP+ADP+AMP Accumulation (nM)
Time (h)
G.
Actin (45 kD)
Panx1 (48 kD)
PARP (116 kD)
cl-PARP (89 kD)
WT Jurkat: hrs post αFas
H.
Actin (45 kD)
Panx1 (48 kD)
PARP (116 kD)
cl-PARP (89 kD)
WT Jurkat: hrs post TS
I.
Actin (45 kD)
Panx1 (48 kD)
PARP (116 kD)
cl-PARP (89 kD)
FADD-def Jurkat: hrs post TS

Figure 1

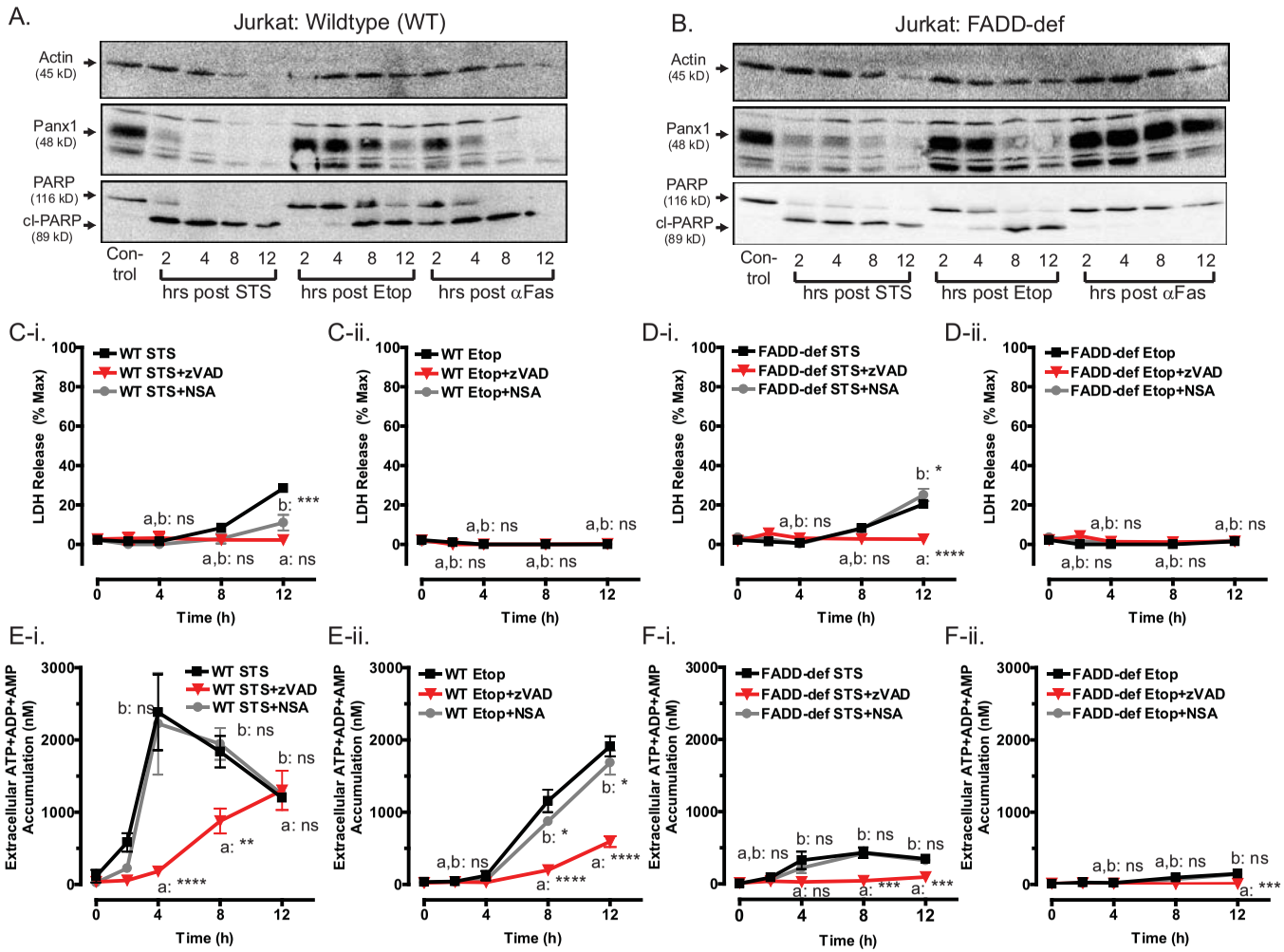
A.
Jurkat: Wildtype (WT)
Actin (45 kD)
Panx1 (48 kD)
PARP (116 kD)
cl-PARP (89 kD)
Con-trol
2 4 8 12 2 4 8 12 2 4 8 12
hrs post STS
hrs post Etop
hrs post αFas
B.
Jurkat: FADD-def
C-i.
C-ii.
D-i.
D-ii.
WT STS
WT STS+zVAD
WT STS+NSA
WT Etop
WT Etop+zVAD
WT Etop+NSA
FADD-def STS
FADD-def STS+zVAD
FADD-def STS+NSA
FADD-def Etop
FADD-def Etop+zVAD
FADD-def Etop+NSA
LDH Release (% Max)
Time (h)
E-i.
E-ii.
F-i.
F-ii.
Extracellular ATP+ADP+AMP Accumulation (nM)

Figure 2

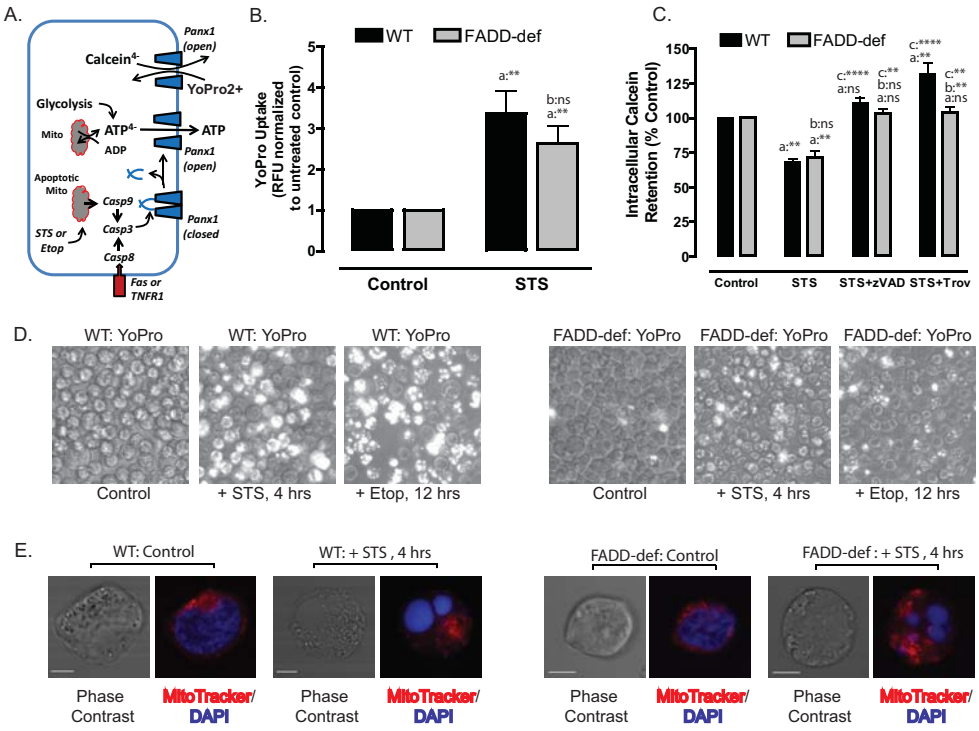
A.
Panx1 (open)
Calcein4-
YoPro2+
Glycolysis
Mito
ATP4-
ATP
ADP
Panx1 (open)
Apoptotic Mito
Casp9
Casp3
Casp8
Panx1 (closed
STS or Etop
Fas or TNFR1
B.
WT
FADD-def
YoPro Uptake (RFU normalized to untreated control)
a:**
b:ns
a:**
Control
STS
C.
WT
FADD-def
Intracellular Calcein Retention (% Control)
Control
STS
STS+zVAD
STS+Trov
D.
WT: YoPro
FADD-def: YoPro
Control
+ STS, 4 hrs
+ Etop, 12 hrs
E.
WT: Control
WT: + STS , 4 hrs
FADD-def: Control
FADD-def : + STS , 4 hrs
Phase Contrast
MitoTracker/ DAPI

Figure 3

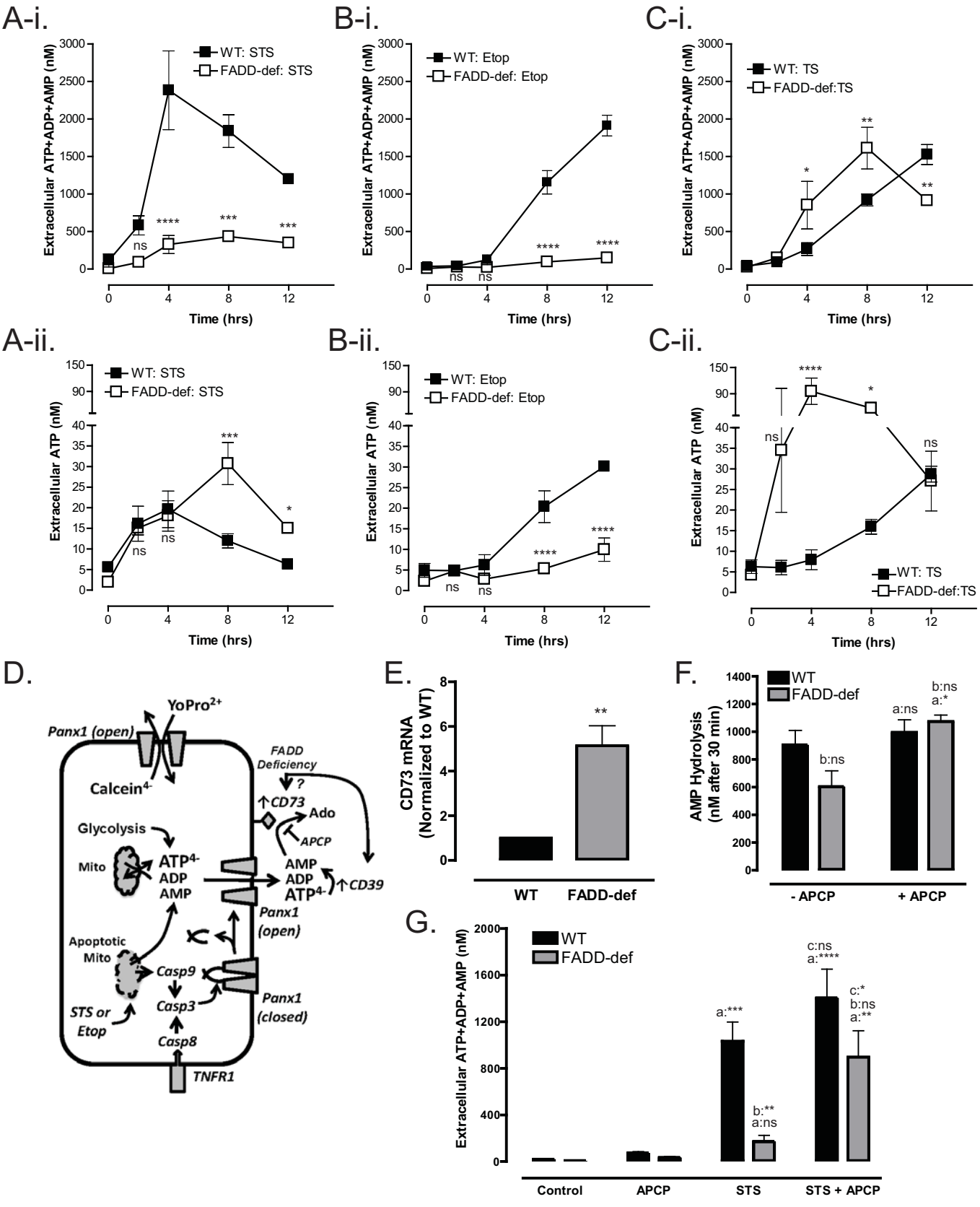
A-i.
B-i.
C-i.
A-ii.
B-ii.
C-ii.
WT: STS
FADD-def: STS
WT: Etop
FADD-def: Etop
WT: TS
FADD-def:TS
Extracellular ATP+ADP+AMP (nM)
Extracellular ATP (nM)
Time (hrs)
D.
YoPro2+
Panx1 (open)
Calcein4-
FADD Deficiency
?
↑CD73
Ado
APCP
Glycolysis
Mito
ATP4-
ADP
AMP
AMP
ADP
ATP4-
↑CD39
Panx1 (open)
Apoptotic Mito
Casp9
Casp3
Casp8
STS or Etop
Panx1 (closed)
TNFR1
E.
CD73 mRNA (Normalized to WT)
WT
FADD-def
F.
AMP Hydrolysis (nM after 30 min)
- APCP
+ APCP
G.
Control
APCP
STS
STS + APCP

Figure 4

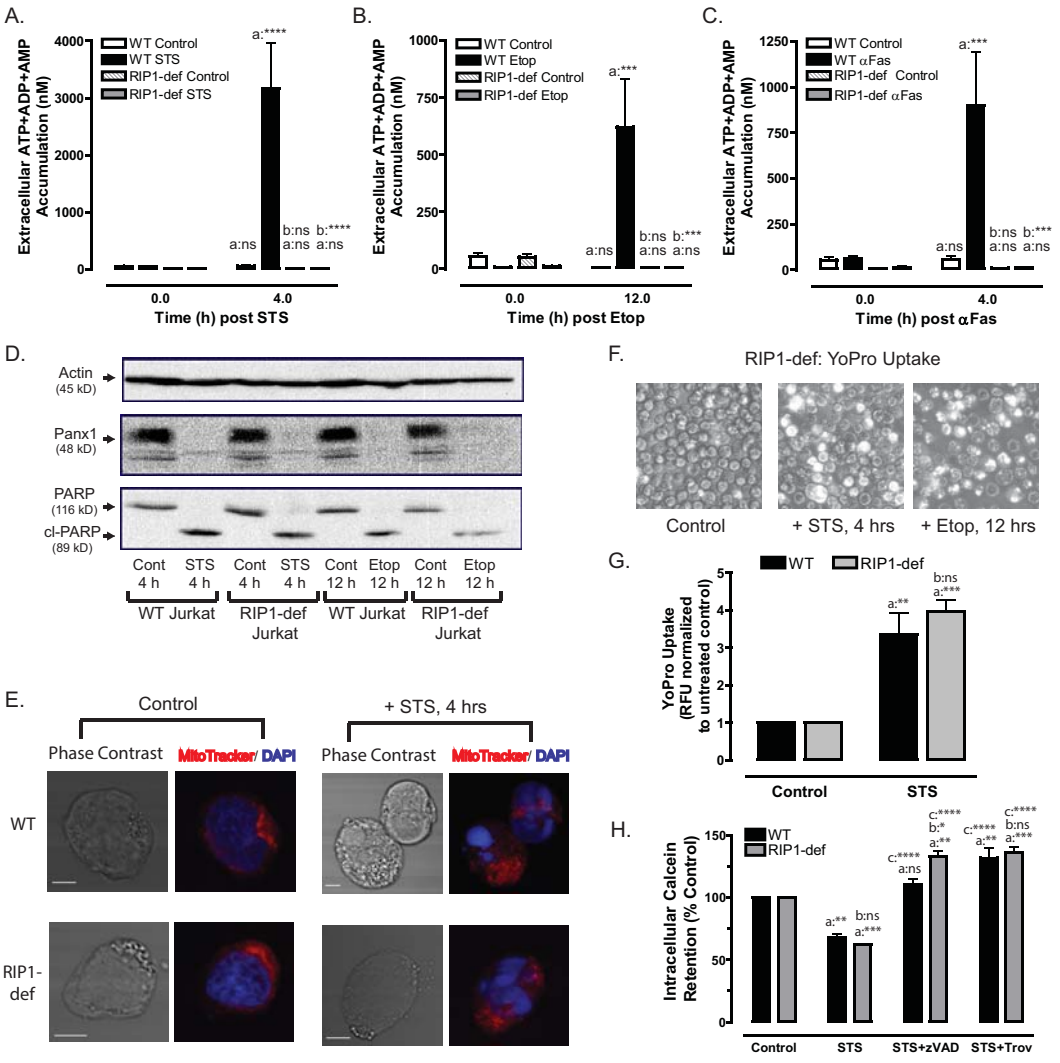
A.
Extracellular ATP+ADP+AMP Accumulation (nM)
WT Control
WT STS
RIP1-def Control
RIP1-def STS
Time (h) post STS
B.
WT Control
WT Etop
RIP1-def Control
RIP1-def Etop
Time (h) post Etop
C.
WT Control
WT αFas
RIP1-def Control
RIP1-def αFas
Time (h) post αFas
D.
Actin (45 kD)
Panx1 (48 kD)
PARP (116 kD)
cl-PARP (89 kD)
Cont 4 h
STS 4 h
Cont 12 h
Etop 12 h
WT Jurkat
RIP1-def Jurkat
E.
Control
+ STS, 4 hrs
Phase Contrast
MitoTracker/ DAPI
WT
RIP1-def
F.
RIP1-def: YoPro Uptake
Control
+ STS, 4 hrs
+ Etop, 12 hrs
G.
WT
RIP1-def
YoPro Uptake (RFU normalized to untreated control)
Control
STS
H.
Intracellular Calcein Retention (% Control)
Control
STS
STS+zVAD
STS+Trov

Figure 5

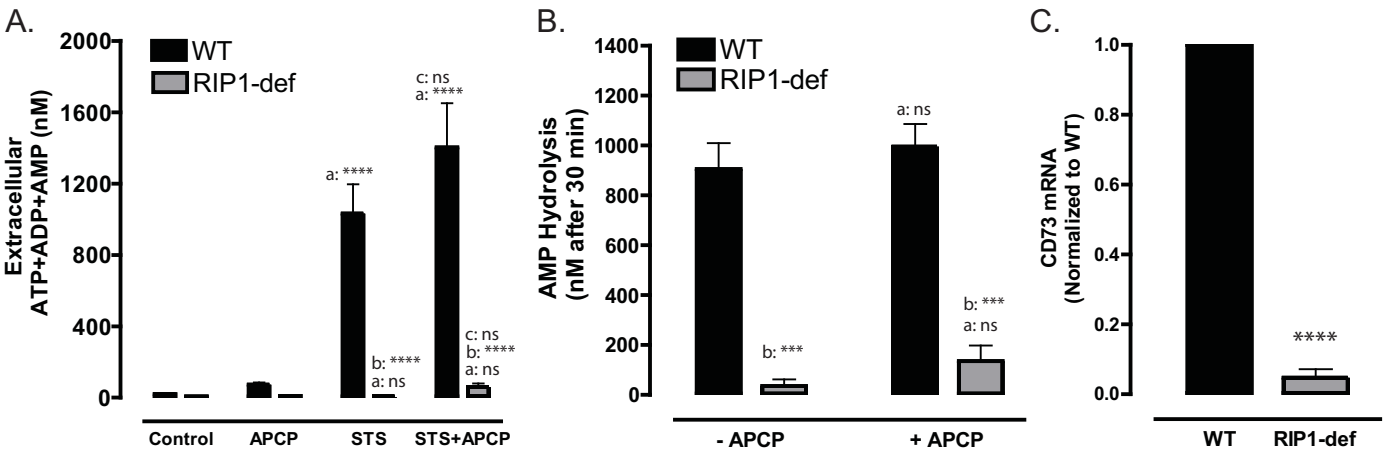
A.
Extracellular ATP+ADP+AMP (nM)
2000
1600
1200
800
400
0
WT
RIP1-def
a: ****
b: ****
a: ns
c: ns
a: ****
c: ns
b: ****
a: ns
Control
APCP
STS
STS+APCP
B.
AMP Hydrolysis (nM after 30 min)
1400
1200
1000
800
600
400
200
0
WT
RIP1-def
b: ***
a: ns
b: ***
a: ns
- APCP
+ APCP
C.
CD73 mRNA (Normalized to WT)
1.0
0.8
0.6
0.4
0.2
0.0
****
WT
RIP1-def

Figure 6

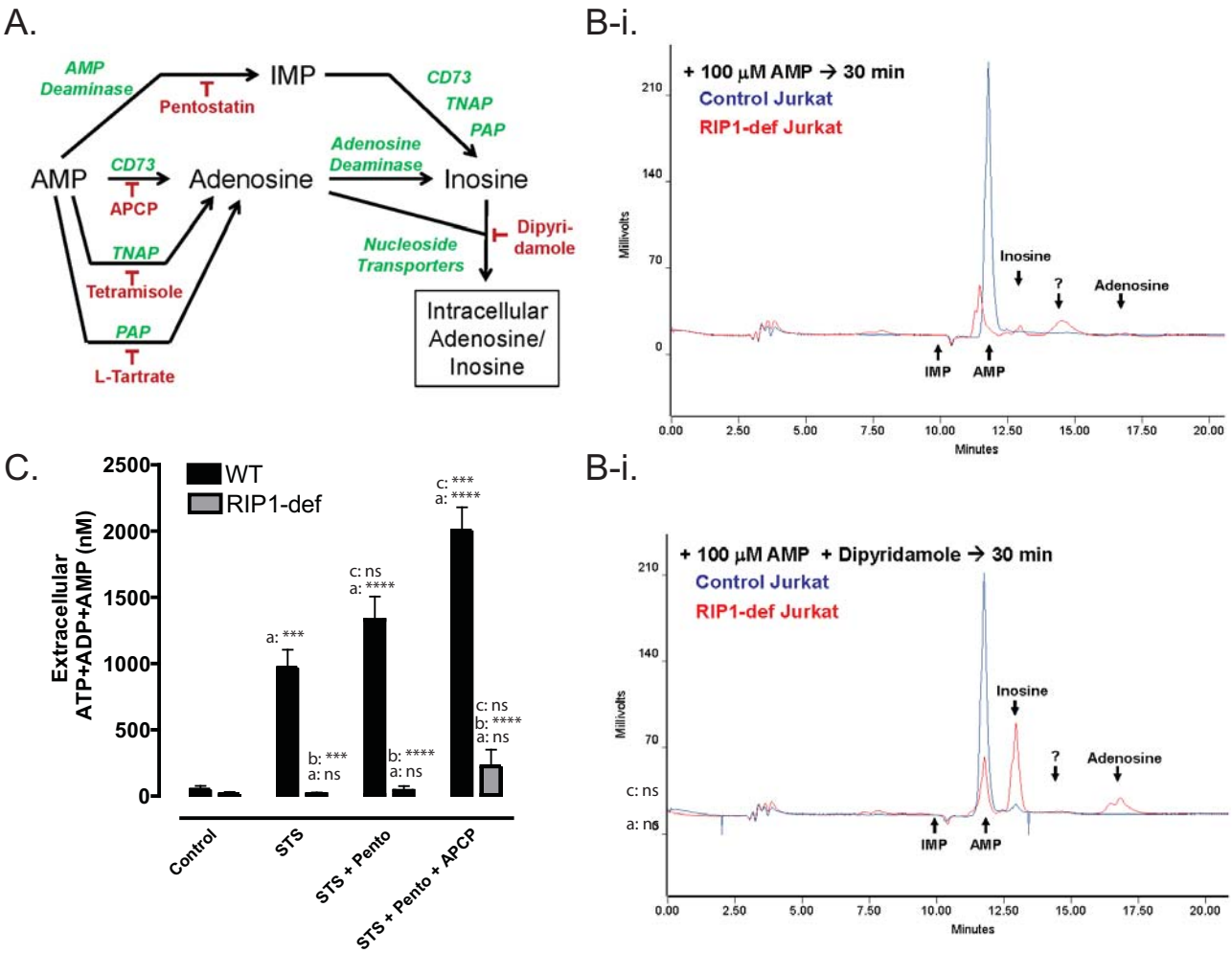
A.
AMP
Deaminase
IMP
Pentostatin
CD73
TNAP
PAP
AMP
CD73
APCP
Adenosine
Adenosine
Deaminase
Inosine
TNAP
Tetramisole
Nucleoside
Transporters
Dipyri-
damole
PAP
L-Tartrate
Intracellular
Adenosine/
Inosine
B-i.
+ 100 μM AMP → 30 min
Control Jurkat
RIP1-def Jurkat
Millivolts
Inosine
?
Adenosine
IMP
AMP
Minutes
C.
WT
RIP1-def
Extracellular
ATP+ADP+AMP (nM)
Control
STS
STS + Pento
STS + Pento + APCP
B-i.
+ 100 μM AMP + Dipyridamole → 30 min
Control Jurkat
RIP1-def Jurkat
Millivolts
Inosine
?
Adenosine
IMP
AMP
Minutes

Figure 7

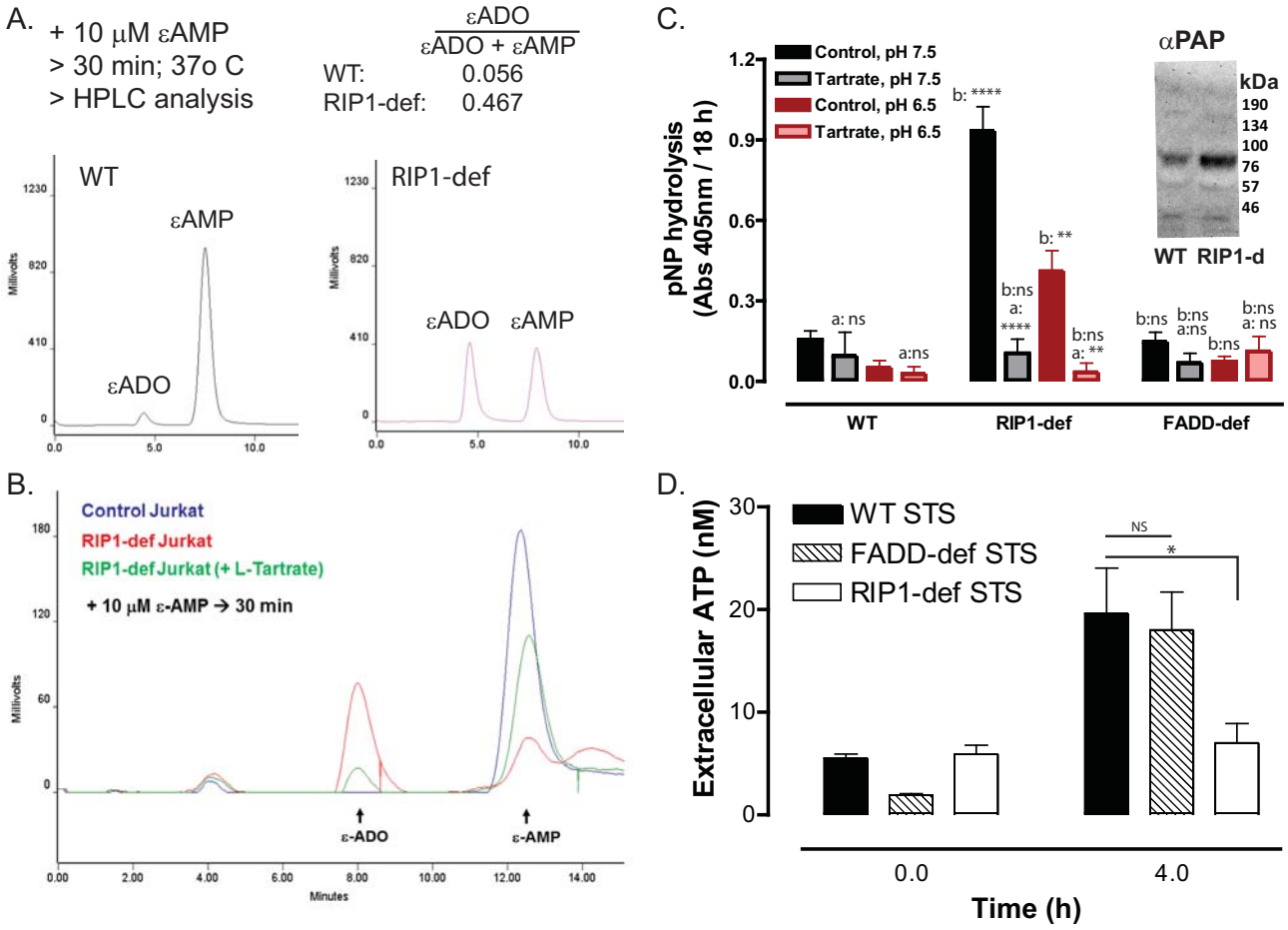
A.
+ 10 μM εAMP
> 30 min; 37o C
> HPLC analysis
εADO / εADO + εAMP
WT: 0.056
RIP1-def: 0.467
WT
εAMP
εADO
RIP1-def
εADO εAMP
Millivolts
Minutes
B.
Control Jurkat
RIP1-def Jurkat
RIP1-def Jurkat (+ L-Tartrate)
+ 10 μM ε-AMP → 30 min
ε-ADO
ε-AMP
C.
Control, pH 7.5
Tartrate, pH 7.5
Control, pH 6.5
Tartrate, pH 6.5
pNP hydrolysis (Abs 405nm / 18 h)
αPAP
kDa
190
134
100
76
57
46
WT RIP1-d
WT
RIP1-def
FADD-def
D.
WT STS
FADD-def STS
RIP1-def STS
Extracellular ATP (nM)
NS
Time (h)

Figure 8